HELSINKI UNIVERSITY OF TECHNOLOGY
Department of Electrical and Communications Engineering
Laboratory of Computational Engineering

Teemu Leppänen

Spatial Pattern Formation in Turing Systems

In partial fulfillment of the requirements for the degree of Master of Science

Supervisor: Academy professor Kimmo Kaski
Instructor: Dr. Mikko Karttunen

Espoo 5th December 2001

TEKNILLINEN KORKEAKOULU DIPLOMITYÖN TIIVISTELMÄ

Tekijä: Teemu Leppänen

Otsikko: Spatiaalinen kuvionmuodostus Turingin systeemeissä

Päivämäärä: 5. joulukuuta 2001 **Sivumäärä:** 66

Osasto: Sähkö- ja tietoliikennetekniikan osasto
Professuuri: S-114, Laskennallinen tekniikka

Valvoja: Akatemiaprofessori Kimmo Kaski
Ohjaaja: Dr. Mikko Karttunen

Tämä diplomityö käsittelee epälineaarisia, Turingin systeemeiksi kutsuttuja reaktio-diffuusiosysteemejä. Brittiläinen matemaatikko Alan Turing ehdotti 1950-luvulla yksinkertaista kemikaalien reaktioita ja diffuusiota kuvaavaa reaktio-diffuusiosysteemiä vastaamaan morfogeneesistä, luonnossa tapahtuvasta kehityksestä. Luonnon monimutkaisuudesta johtuen tutkijat eivät ole toistaiseksi onnistuneet kehittämään Turingin systeemiin perustuvaa mallia, joka varsinaisesti kuvaisi morfogeneesiä, vaikka eläinten nahan ja turkin värityksen mallintamiseen Turingin systeemejä onkin käytetty.

Turingin systeemit ovat kuvionmuodostuksen kannalta erittäin monipuolisia, mikä tarkoittaa, että ratkaisemalla numeerisesti näitä matemaattisesti määriteltyjä systeemejä saadaan aikaan monenlaisia spatiaalisia kuvioita kahdessa ulottuvuudessa ja rakenteita kolmessa ulottuvuudessa. Nämä vaihtelevat täplistä raitoihin ja lamelleista kaoottisiin rakenteisiin. Tässä diplomityössä esitetään tuloksia kolmiulotteisista Turing-systeemeistä, joita ei ole aiemmin numeerisin simulaatioin tutkittu.

Esittelemme kolmiulotteisen Turingin systeemin perusominaisuuksia ja vertaamme näitä kaksiulotteiseen systeemiin. Huomaamme, että morfologisesta kehityksestä tulee entistä kiinnostavampaa ja monimutkaisempaa kolmessa ulottuvuudessa. Siirtymä kahden ja kolmen ulottuvuuden välillä on erityisen kiinnostava.

Motivaatiomme Turingin systeemeiden tutkimiseen on biologinen. Näytämme, miten tiettyjen pisteiden välille voidaan kasvattaa yhteyksiä käyttämällä Turingin systeemiä, jossa on kemikaalien lähteitä. Verkostolla, joka tällä tavoin syntyy, on monia kiinnostavia ominaisuuksia, ja ehdotammekin Turingin systeemistä ja aktiivisatunnaiskävelijämalleista yhdistettyä kokonaisuutta selittämään neuroverkon muodostumisen keskeisiä piirteitä eli sitä, miten hermosolut eli neuronit löytävät yhteyksiä toisiin neuroneihin.

Avainsanat: Turingin systeemi, reaktio-diffuusioyhtälö, kuvionmuodostus

HELSINKI UNIVERSITY OF TECHNOLOGY

ABSTRACT OF THE MASTER'S THESIS

Author: Teemu Leppänen

Title: Spatial Pattern Formation in Turing Systems

Date: 5th December 2001 **Number of Pages:** 66

Department: Electrical and Communications Engineering

Professorship: S-114, Computational Engineering

Supervisor: Academy Professor Kimmo Kaski

Instructor: Dr. Mikko Karttunen

This thesis concentrates on nonlinear dynamical reaction-diffusion systems called Turing systems. In the 1950s British mathematician Alan Turing proposed a simple reaction-diffusion system describing chemical reactions and diffusion to account for morphogenesis, i.e., development in nature. Due to the complexity of nature, researchers have not yet succeeded in developing a Turing system based model that would describe morphogenesis in essence, although specific examples such as the skin and coating coloring of animals have been modeled using Turing systems.

Turing systems show a very rich behavior from the pattern formation point of view, which means that by numerically solving these mathematically defined systems we obtain a variety of spatial patterns in two dimensions and structures in three dimensions, varying from spots to stripes and from lamellar to chaotic structures. In this thesis we present results of a three-dimensional system, which has never before been studied using numerical simulations.

Due to the unique nature of our results we introduce some basic characteristics of the three-dimensional Turing system and compare the system with a two-dimensional one. We notice that the morphological development becomes more interesting and complex in three dimensions. The transition between two and three dimensions is especially interesting.

Our motivation for studying the Turing systems is biological. We show how connections between certain points can be grown by using a Turing system with sources of chemicals. The resulting connected network has many interesting properties, and we propose a combined Turing system and an active random walker model to explain some salient features of neural patterning, i.e., how neurons establish connections to other neurons.

Keywords: Turing system, reaction-diffusion, pattern formation

Foreword

The research presented in this thesis has been carried out in the Laboratory of Computational Engineering at the Helsinki University of Technology, mainly during summer and fall 2001, while working as a member of the biophysics and statistical mechanics group.

First and foremost, I would like to thank my supervisor Academy Professor Kimmo Kaski for introducing me to the interesting research topic of Turing systems as I stumbled through the doors of the LCE after my second year of studies. In addition, I wish to thank him for providing excellent working conditions. In my mind, the LCE offers unbeatable framework for carrying out top-notch research and I look forward to continuing work at the LCE.

I wish to express my gratitude to my instructor Dr. Mikko Karttunen for his uncompromising attitude to make this thesis as good as it can be, but not any better. I don't think that I ever asked him a question he could not answer, which in my opinion does not reflect only the stupidity of the questioner, but also the talent of the respondent.

I wish to thank Professor Rafael A. Barrio of Mexico for inspiring guidance into the jungle of nonlinear dynamics. I would also like to thank him for the hospitality and relaxed atmosphere during my visit to the Department of Theoretical Physics at the University of Oxford.

I would like to thank all the personnel of the LCE for making the laboratory a very pleasant environment. In particular, I would like to thank my roommates Sebastian and Ville for tolerating me for the last 18 months. In addition, I thank them for advice and encouragement. Also the other dudes, Ilkka, Jari, Marko, Markus, Petri, Toni and the other Ville, deserve a mention.

I thank all my friends out of the LCE for being a counterbalance to studies and work.

I wish to express my deepest gratitude to my wonderful parents and my delightful sisters for taking such a good care of me throughout my studies at HUT.

Lastly, thank you Satu for your love, appreciation and understanding.

Otaniemi, 5th December 2001

Teemu Leppänen

Contents

List of Figures

Abbreviations and notations

$\vec{X}$	state of a system
T	temperature
ω	angular velocity
t	time
D/D_x	diffusion coefficient for chemical x
x_t	time derivative of chemical concentration x
Ω	subdomain of a space
h	lattice constant (dx)
δ	time step (dt) / diffusion coefficient
$\vec{k}$	wave vector
k	wave number
LCE	Laboratory of Computational Engineering
u, v	concentrations of chemicals
α, β, γ	phenomenological parameters
r_1, r_2	adjustment parameters
F	feeding parameter for chemical U
K	rate constant for chemical V
(u_0, v_0)	steady state of a system
f_u, f_v, g_u, g_v	partial derivatives evaluates at (u_0, v_0)
λ	eigenvalue of the linearized problem
$\eta(\vec{x}, t)$	random noise
$\delta(\vec{x})$	Dirac delta function
$C_n(\vec{x}, t)$	n point correlation function
$S(k, t)$	structure factor

Chapter 1

Introduction

Nature presents many fascinating questions by showing a great diversity of patterns in plants, animals and other natural formations. Several examples can be found. One could consider the veins of a tree leaf, the vascular system of a human being, lightning caused by a thunderstorm, the development of branches of a tree, the growth of the limbs of primates and the formation of the delta of a river. Although the connection between the above phenomena seems superficial and they do not appear to be linked in any way, there is an increasing interest in developing simple and plausible mathematical models that could be generalized to model as many different ways of nature as possible.

The impetus for this was given by the famous British mathematician Alan Turing [Turing, 1952]. In his seminal article, *The Chemical Basis of Morphogenesis*, he claimed that a simple system of coupled reaction-diffusion equations could give rise to spatial patterns due to a phenomenon called diffusion-driven instability provided that certain conditions for parameter values were met. He also proposed that this model could explain morphogenesis, i.e., the development from an embryo to an animal – or from a seed to a plant. It is well established that DNA is an essential part of the development since it contains the blue-print for the development but it is not fully known how nature reads DNA. Turing suggested that the formation of spatial patterns is based on the information contained in DNA and that patterns specify the tasks for the cells.

Turing died just two years after he had published the paper, which was groundbreaking for both the biological merits and the fact that diffusion could act as a

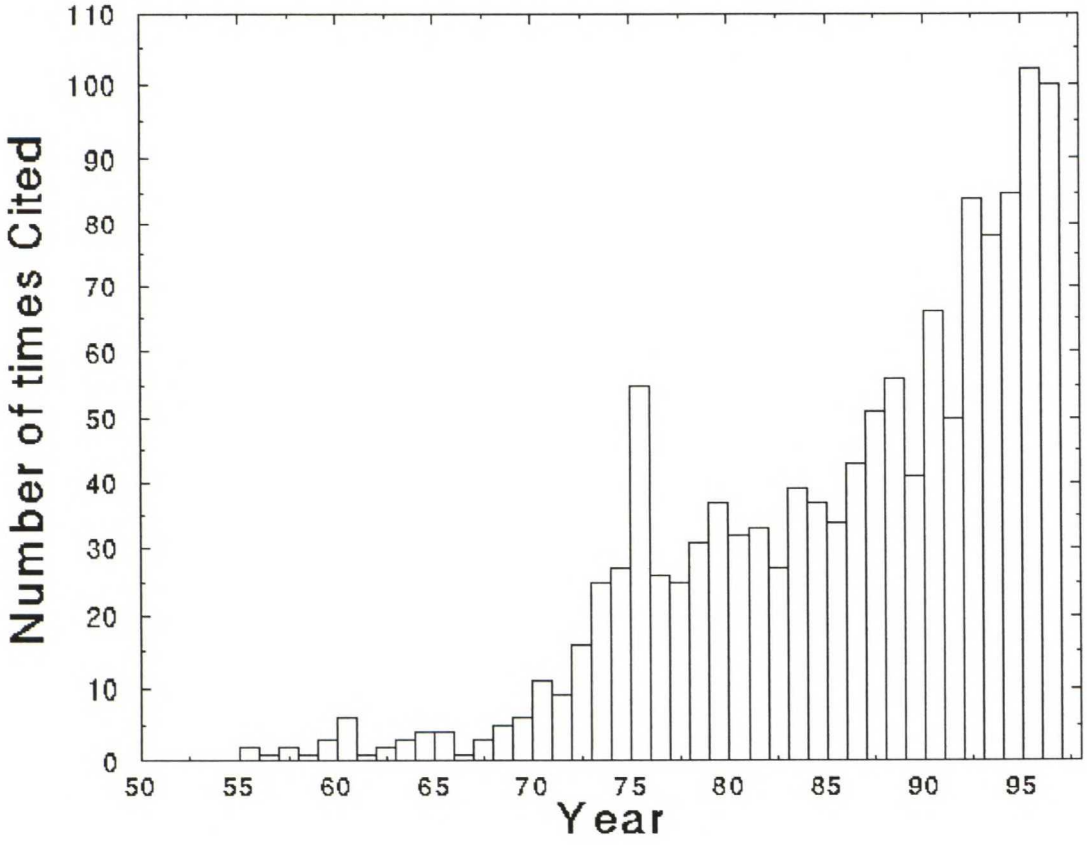

Figure 1.1: The citation histogram [Pearson, cited 26.7.2001] of Turing's article *The Chemical Basis of Morphogenesis* [Turing, 1952]. At the time of publications the results were controversial and were overlooked for a long time. Since the 1970s there has been rapidly increasing interest in Turing's ideas. Notice that the envelope curve of the diagram is nearly exponential.

destabilizing factor. Although Turing's ideas were adopted slowly by the scientific community, as can be seen from Figure 1.1, his work had a great impact on the modern nonlinear dynamical theory.

Nonequilibrium physics and pattern formation is a vast field of science. This thesis concentrates on reaction-diffusion systems and their pattern formation properties. A reaction-diffusion system consists of substances that diffuse and react, i.e., spread over the domain and interact mutually, this interaction being typically nonlinear. Models of such systems can be used to describe various chemical reactions involving two or more chemicals with different properties, e.g. the boiling of pulp. On a larger scale, reaction-diffusion models have been used e.g. for studying the spreading of

forest fires [Provatas et al., 1995, Karttunen et al., 1997].

In this thesis we will study two different reaction-diffusion systems, both containing nonlinear interactions. The first system is a general Turing system obtained by a Taylor expansion around the stationary state [Barrio et al., 1998]. The conditions for the diffusion-driven instability to occur will be derived and the desired growth modes will be isolated using linear analysis. The results show how the morphological development can be directed by adjusting the parameters and initial conditions. The second model we study is the well-known Gray-Scott model [Gray and Scott, 1983], which shows very complex spatiotemporal behavior. It will be shown that in the presence of sources of reacting chemicals described with a certain set of parameters this model will generate tubular structures connecting the sources.

Due to the form and time-dependent nature of the Turing systems, analytical solutions to these equations do not usually exist. In practice, this means that the continuous system must be discretized and solved numerically using computer simulations. The rapid development of computers has made simulations of these systems less troublesome and the research has progressed rapidly. There are also many experiments made with reacting chemicals that confirm, explain and enlight the physical basis which should never be forgotten while doing the computer simulations.

In this thesis the approach is based more on statistical physics and pattern formation rather than biology. However, the biological interpretations will be discussed in suitable contexts. The goal is to introduce the reader to nonlinear dynamical theory and to present new results of three-dimensional Turing systems. So far, these systems have only been solved and analyzed in two dimensions. It will be shown that the pattern formation is significantly affected by the spatial dimensionality of the system and hence very complex structures are obtained at higher dimensions than two.

The thesis will proceed as follows: Chapter 2 will concentrate on the general aspects of pattern formation. Chapter 3 is about numerical methods needed for solving the systems, computational details and visualization. In Chapter 4 the general Turing model will be introduced, analyzed and simulated. Chapter 5 will present the derivation and analysis of the Gray-Scott model and results obtained for a three-dimensional model. Finally, Chapter 6 is reserved for discussion and conclusions.

Chapter 2

Theory of Pattern Formation

In this chapter, we will introduce some of the most important concepts related to pattern formation. The definitions are theoretical and after introducing each concept we consider the meaning of it in a Turing system. Finally, we present three important experiments which strengthen the background of the theory.

There exist many comprehensive books and a great number of review articles on this topic. The book *Mathematical Biology* [Murray, 1993] offers a wide view to the possibilities of modeling nature. *Introduction to Nonlinear Science* [Nicolis, 1995] gives an introductory, yet precise approach to the topic. *The Dynamics of Patterns* [Rabinovich et al., 2000] is more like a versatile reference book for professionals and it has an essential chapter about the key experiments in pattern formation. The exhaustingly long, but comprehensive article *Pattern Formation Outside of Equilibrium* [Cross and Hohenberg, 1993] is a fundamental reference in the field.

2.1 Terms and concepts

2.1.1 Nonequilibrium vs. equilibrium

The pattern formation related research belongs to the field of nonequilibrium statistical physics. However, many of the studied models are phenomenological and do not have direct connection to microscopics. For example the Turing systems could be considered as a coarse-grained model of microscopic level properties of chemicals.

By coarse-graining we mean increasing the time and length scales at which we study the system. In a Turing system this means that we do not describe every atom separately, but approximate the behavior by a concentration field.

The concept of thermodynamical equilibrium is defined by four conditions. First, the system must be in mechanical equilibrium, i.e., the sum of forces and momenta in the system must be zero. Second, the system must be in chemical equilibrium implying that the chemical potential must be constant. Third, the system must be in thermal equilibrium, i.e., the temperature must be constant. And fourth, the distribution of states must be well defined, i.e., the particles must obey Maxwell-Boltzmann statistics. The above conditions are a restatement of the zeroth law of thermodynamics that stipulates that if system A is in equilibrium with B and C, then B is in equilibrium with C. If the four conditions are not met, the system is in a nonequilibrium state.

2.1.2 Dissipative vs. conservative

Dynamical systems can be divided into two classes, conservative and dissipative systems. Conservative systems conserve the measure of the phase space, whereas the dissipative systems tend to evolve to a subset of phase space with zero volume. If the system is defined by

$$\frac{d\vec{X}}{dt} = \vec{F}(\vec{X}, \lambda), \tag{2.1}$$

then a conservative system would satisfy the condition $\nabla \cdot \vec{F} = 0$ and a dissipative system would satisfy $\nabla \cdot \vec{F} < 0$. One should note that the inequality can be defined also to the other direction. In general, one talks about nonconservative systems as $\nabla \cdot \vec{F} \neq 0$. However, the systems with $\nabla \cdot \vec{F} > 0$ are not of great interest, due to the fact that their phase space expands and they escape to infinity, which is not a physical situation.

Turing systems and most of the other systems describing pattern formation are dissipative. This can be easily understood by observing the time evolution of Turing system, which starts with substantial changes in the morphology and ends with infinitesimal changes, i.e., at the end the subset of the phase space the system explores is very small.

2.1.3 Stability

Stability of a system deals with the response to perturbations. Let us denote the state of the system by $\vec{X}_s$ and a time-dependent perturbation by $\vec{x}(t)$. In nature, the perturbations are manifested for example in the form of thermodynamic fluctuations, and a system never stays in a single state forever, but it explores the phase space available to it. We can write an equation for the real state $\vec{X}(t)$ of the system as

$$\vec{X}(t) = \vec{X}_s + \vec{x}(t) \tag{2.2}$$

The objective of the stability analysis is to investigate whether the system stays close to the state $\vec{X}_s$ or disperses far from it as time proceeds.

Two different kind of stabilities can been defined. Here we follow the definitions of Nicolis [1995]. It is said that the state $\vec{X}_s$ is stable in the sense of Lyapunov if a perturbed system never deviates "very far" from $\vec{X}_s$. On the other hand, a system is said to be asymptotically stable if it satisfies the previous statement, and in addition, the perturbed system tends to return to the original state $\vec{X}_s$ as time goes on. An asymptotically stable system is also stable in the sense of Lyapunov, however, the opposite is not always true. If a system is not stable, it is said to be unstable.

Stability can be defined mathematically as follows: if one defines a norm $\|\cdot\|$ in the phase space and denotes the point where the system is perturbed to $\vec{X}_0$, we can state that a system is stable in the sense of Lyapunov if

$$\forall\ \epsilon > 0\ \exists\ \delta(\epsilon) > 0\ s.t.\ \forall\ \vec{X}_0,\ \|\vec{X}_0 - \vec{X}_s\| < \delta\ \Rightarrow\ \|\vec{X}(t) - \vec{X}_s\| < \epsilon\ \forall\ t \geq 0.$$

The system is asymptotically stable if, in addition, $\|\vec{X}(t) - \vec{X}_s\| \to 0$ as $t \to \infty$.

Although these ideas can be defined mathematically and explained by using the phase space and its states, the idea of stability is intuitive: If we disturb a system by a small amount, an asymptotically stable stable system returns back to its original state. For example, a pendulum is asymptotically stable as a result of the gravitational forces. In a weightless environment it would not be, because the pendulum would just float in the air randomly until the air resistance would stop the movement.

As an example of an unstable system one could consider an empty cylindrical metal-

lic soda can which is under axial stress (e.g. the can is on the ground and you are pressing it with your foot). Now, if you hit simultaneously on the opposite sides of the can, it collapses under the pressure, i.e., a small perturbation results in the destruction of the can.

The final patterns and structures generated by a Turing system are stable states, because the Turing system evolves in time as long as it finds a stable state. However, our simulations are not infinitely long and thus we cannot conclude without any doubt whatsoever that the structures generated by the Turing system are stable. Anyway, we can test the stability by adding noise and we will do this in Chapter 4.

The robustness or stability of a certain structure depends on the amplitudes of the unstable wave vectors forming it. Due to the quadratic nonlinear term the amplitude is almost two orders of magnitude greater for the spherical structures than for the lamellar structures (stripes). As it will turn out in Chapter 4, the spherical structures are much more stable against noise. If a significant amount of noise is added to the two structures discussed above, in the case of spherical structures the chemical waves act as carriers for the noise, whereas in the case of lamellar structures, the chemical wave is modulated to the noise signal and the chemical information is lost.

The stability of a system can be studied by using a linear analysis. In the linear analysis the behavior of the system is studied by expanding the equations of motion using a Taylor series and writing equation for the perturbation, where all the nonlinear terms of the series have been dropped out. This analysis tells which states are stable and which are unstable and it can be used for mode selection, choosing the characteristic scale of the system by adjusting parameter values. Both Cross and Hohenberg [1993] and Nicolis [1995] describe the method in detail. We will apply linear analysis in Chapters 4 and 5.

2.1.4 Symmetry breaking

Symmetry is one of the central concepts in statistical physics and in pattern formation. Typically, transitions between different states in a system are related to changes in the symmetry properties, e.g. the system may experience a symmetry breaking transition. Below, we will discuss symmetry and its importance in nature.

Let us define two different spatial symmetries, translational symmetry and rota-

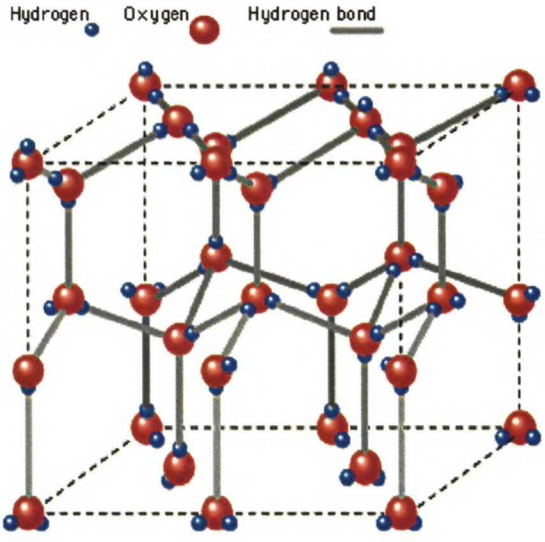

Figure 2.1: The hydrogen bonds fix the crystal structure in the ice. In warm water the thermal fluctuations of water molecules keep the fluid homogeneous. Water is one of the few substances that expand in the solid state. The figure is from [Devlin, cited 15.11.2001].

tional symmetry. As an illustrative example of symmetry breaking we can consider the fluid-solid transition. Neglecting the effects of surfaces, a fluid is rotationally invariant and spatially homogeneous. Translational invariance is implied by the fact that the average properties of the liquid are independent of any arbitrary translation in the system, and rotational invariance by the fact that the average properties remain independent of any rotation about any axis. These properties are reflected by the following two properties of the radial density profile ϕ: 1) It remains unchanged as one moves to the direction of any vector $\vec{r}$, i.e., $\langle\phi(\vec{x})\rangle = \langle\phi(\vec{x}+\vec{r})\rangle$, and 2) the rotational symmetry is manifested by the uniformity of ϕ.

The liquid-solid transition involves a symmetry breaking. Consider water which is cooled down. As the temperature decreases below zero degrees centigrade, the water molecules become organized and form a crystalline solid, since the thermal energy no longer dominates over the energy of hydrogen bonds, which fix the ice crystal. Figure 2.1 shows the structure of ice. The crystal is less symmetric, but it is more ordered. Due to the fact that the radial density profile is not constant irrespective of any amount of rotation, the crystal is not rotationally symmetric.

However, the crystalline ice is not completely without symmetry, it has discrete symmetry. Indeed, the discrete translational symmetry is demonstrated by the fact

that if we can make translations that are multiples of the lattice constant, i.e., the characteristic length of the crystal lattice. In addition, discrete rotational symmetry is established if while rotating we consider only a set of discrete angles.

As a second example we will consider a two-dimensional Ising model. It will help us to define another central concept in pattern formation, namely the order parameter. Ising model is one of the most important models in the studies of phase transitions. The model describes a ferromagnet with help of a lattice where on each site the spins point either up or down.

Symmetry breaking can be described more quantitatively by defining an order parameter, which is a quantity that describes the degree of order in the system. On one side of a transition the order parameter is zero and on the other side nonzero. For example, in the Ising model the order parameter is the degree of magnetization $|\langle \vec{m} \rangle|$ in the system. It should be noticed that there is no unique way of defining an order parameter, but each system must be considered separately.

Figures 2.2a-d describe the behavior of the spins in the Ising model and Figure 2.3 shows the phase diagram, i.e., the order parameter as a function of temperature. In the absence of external fields and at high temperature, there is no net magnetization in the system. As the temperature is lowered, there exists a critical temperature (Curie temperature) T_C at which the magnetization start to grow from zero. In the high temperature phase, the system is disordered, i.e., there is no preferred direction in the system. Furthermore, if we assume periodic boundary conditions, we can say that the system is completely symmetric in a statistical sense.

In the low temperature phase, i.e., as T becomes lower that T_C the system starts to become ordered. Small ordered domains start to form, and thus the net magnetization increases from zero. The system starts to gain order and the completely symmetric disordered state becomes ordered, but of lower symmetry. The low temperature phase is called the broken symmetry phase.

How do the above concepts relate to Turing systems? Morphogenesis, by the definition of the word is about formation and growth of patterns. Turing noticed that in the development of an embryo, it is in the early stages symmetric, but as time progresses this symmetry disappears as the embryo starts to develop some structure. Turing asked the question, what is the mechanism that causes the symmetry breaking? Thus, symmetry breaking lies at the heart of pattern formation.

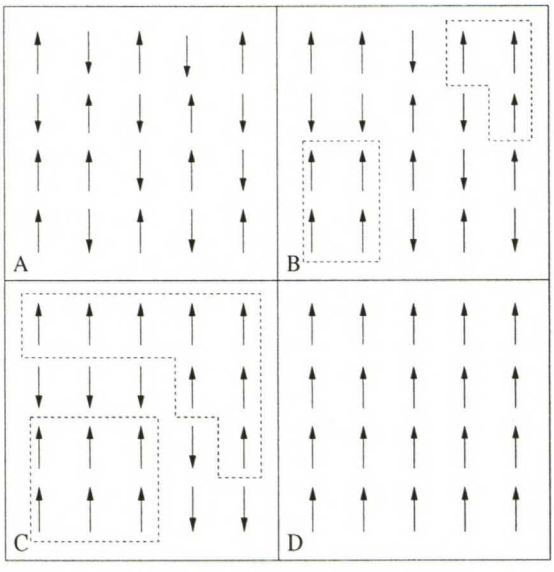

Figure 2.2: The alignment of spins in the plane in two-dimensional Ising model. In the figure a the temperature is above the Curie temperature, $T > T_C$. As the temperature is decreased below T_C, ordered domains start to appear. At $T = 0$K all the spins become aligned.

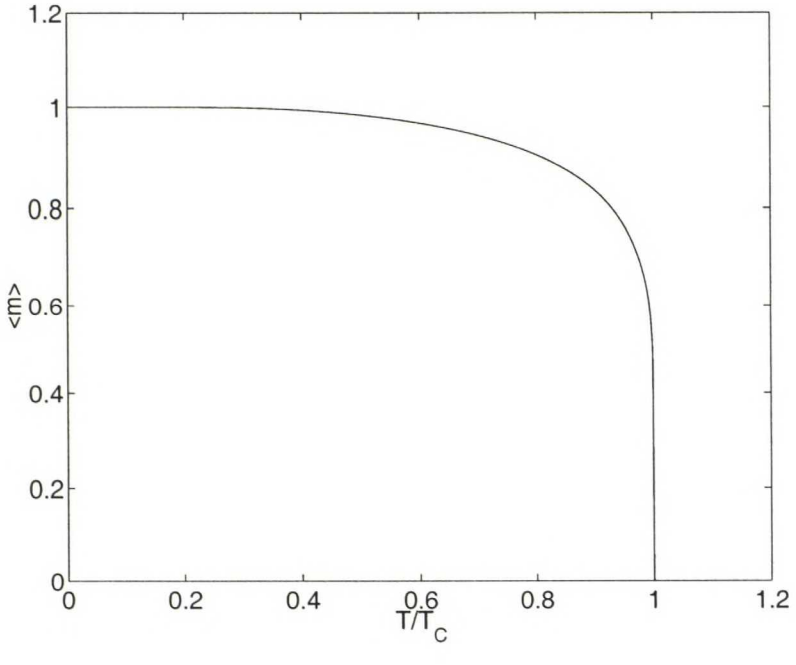

Figure 2.3: The net magnetization as a function of normalized temperature. The magnetization saturates as the temperature approaches zero.

2.1.5 Bifurcation

In equilibrium thermodynamics and statistical mechanics we have phase transitions as discussed above in the cases of the liquid-solid transition and the Ising model. In systems out of equilibrium bifurcation can be understood as a change in the state of a system. Generally speaking, one could say that the symmetry of the system breaks as a bifurcation takes place. The word bifurcation is used for nonequilibrium systems and it is analogous to phase transition in equilibrium systems. Bifurcations can be classified according to the terms determining the reactions to saddle-node, transcritical, pitchfork and Hopf bifurcations. The pitchwork bifurcation is divided to supercritical and subcritical bifurcations corresponding to second-order continuous transition and first-order discontinuous transition, respectively. There is a comprehensive review article by [Cross and Hohenberg, 1993], which discusses the bifurcation in detail.

2.2 Fundamental experiments

In the following we will shortly present three important experiments, which illustrate some of the most important features of pattern formation, i.e., competition between driving forces and dissipation of energy. These experiments are very important in the sense that they combine mathematical models to real physical situations.

2.2.1 Faraday experiment

In the first half of the 19th century English chemist and physicist Michael Faraday studied magnetic fields. He noticed that there were similarities in the field induced by a magnetic pole and vibrations on the surface of a thin layer of water with which he had been experimenting earlier [Faraday, 1831]. Faraday is considered to be one of the greatest experimentalists ever lived and next we will consider his experiment with water, although his other works may even be more important to science in general.

Faraday experiment is carried out by pouring a liquid uniformly onto a horizontal Petri dish. The height h of the liquid layer must be small compared to the dimensions of the dish. Then the dish is vibrated using a vibrator governed by $A(t) = A\sin(\omega t)$,

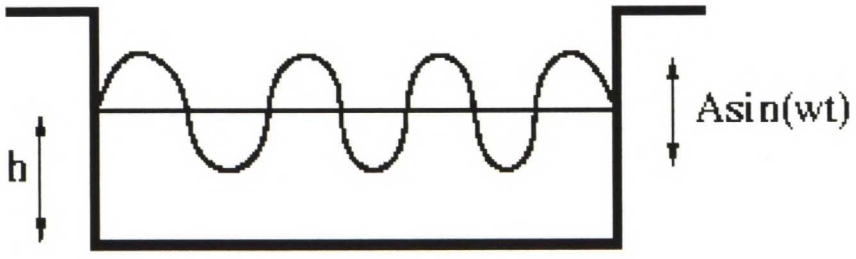

Figure 2.4: The experimental setup in Faraday experiment. The height of the liquid layer is h and the vibrator (underneath the dish) is governed by $Asin(\omega t)$. Numerical values could be for example $h = 2mm$, $A = 50\mu m$ and $\omega = 10rad/s$ (from [Barrio et al., 1997]).

where A is the amplitude and ω the angular frequency. Depending on the amplitude and frequency, different kind of patterns can be observed on the surface of the water. A qualitative view of the experimental setup is presented in Figure 2.4.

In the original experiment Faraday observed two- and fourfold symmetries. Later pentagonal, octagonal and dodecagonal symmetries have been observed. Recently it has been shown by Barrio et al. [1997] that the symmetries can be chosen by adjusting the frequency of the vibrations when a special liquid with a low kinematic viscosity and large density is used. Figure 2.5 shows some of the results of these experiments. In addition, they proposed that the development of the surface pattern as the amplitude and frequency were increased resembled the evolutionary development of sea urchins, a species that has lived millions of years ago and lives today. As the amplitude was further increased, they obtained a chaotic pattern (Figure 2.5d). Barrio et al. [1997] derived a theoretical model to describe the shape of the surface, compared the model and experiments, and showed that this nonlinear model is analogous to Turing systems, which may have complex diffusion coefficients.

In the Faraday experiment the symmetry breaking can be understood as follows: At first, there is a uniform layer of the liquid, i.e., a perfectly symmetric situation. Applying external forces (vibrations) to the system results in an asymmetric situation in the sense that the layer is not uniform anymore, i.e., the surface is not flat. Thus we end up to an asymmetric situation starting from a symmetric one.

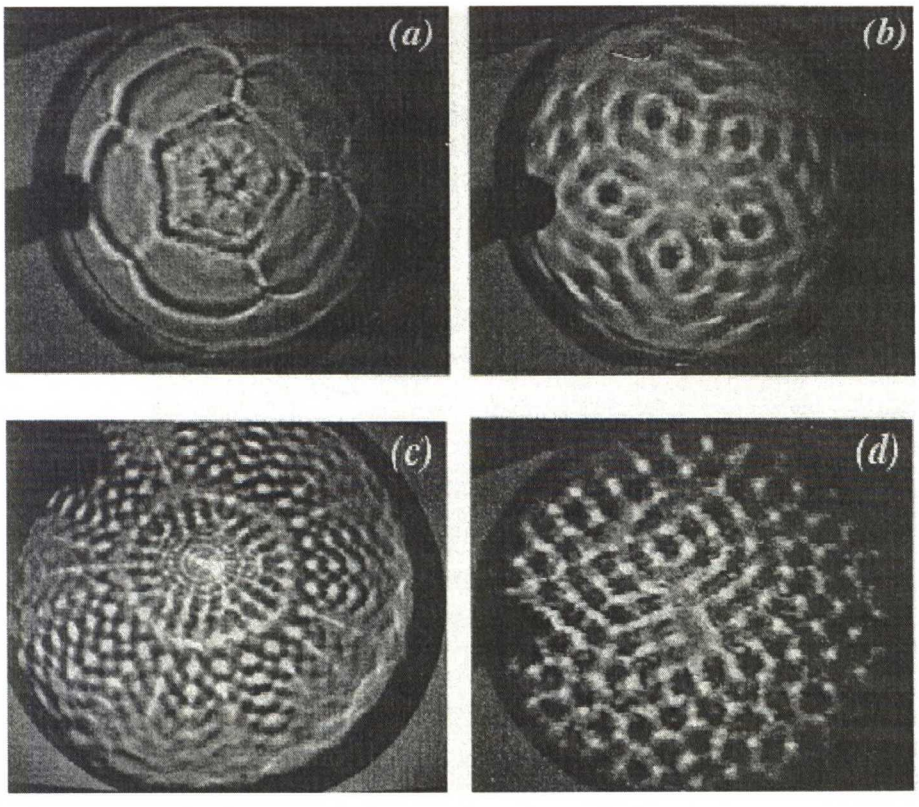

Figure 2.5: Surface patterns obtained in Faraday experiment by using a liquid with high density and low kinematic viscosity. The camera is straight above the dish. The frequency and amplitude of vibration is increased through figures a-d. The shown development resemble evolutionary development of sea urchins. The pattern in the figure c corresponds to the shape of present sea urchins. Reproduced from [Barrio et al., 1997].

2.2.2 Rayleigh-Bénard convection

The Rayleigh-Bénard experiment concerns the problem of thermal convection and was first performed by Bénard [1900]. It was not until sixteen years later, when Lord Rayleigh tried to explain the phenomenon theoretically [Rayleigh, 1916]. Although the experimental setup itself is simple, it displays very rich behavior. In everyday life, examples of thermal convection related to this experiment are the circulation of water in atmosphere and in the oceans due to weather changes, and the motion of continental plates caused by movements of magma in the mantle of the earth.

The idea of Rayleigh-Bénard convection is illustrated in Figure 2.6. Consider a fluid placed between two infinite parallel horizontal plates assumed to be perfect heat conductors. We denote the temperature of the lower plate by T_1 and the upper plate by T_2, and the temperature difference between the lower and upper plates by $\Delta T = T_1 - T_2$. If $\Delta T < 0$, there will be net motion in the fluid. If ΔT is positive, but small the thermal conduction from lower to upper plate takes place and the temperature profile between T_1 and T_2 becomes linear. The fluid will remain at rest since the viscosity and thermal conduction are able to stabilize the system against small perturbations: viscosity generates internal friction opposing movement and dissipative effects of thermal conduction tend to restore the displacements.

As the ΔT exceeds a certain threshold ΔT_c, thermal expansion causes the fluid near the lower plate to be substantially less dense than the colder fluid above, which is an unstable situation in gravitational field. The warmer fluid near the lower plate wants to rise, but there is no space for it above. Thus some of the colder molecules must move down due to conservation of mass and make space for warmer molecules. This fixes a finite wave length for the instability, the wave length meaning the width of the formed convection cells. This is clearly visible in Figures 2.6 and 2.7.

As a molecule moves upwards, it is cooled down and as a result it falls back down. Convection cells are called Bénard cells and the fluid will start moving up and down in a circular fashion. Figure 2.6 shows a qualitative view of Bénard cells. Clearly, the resulting situation is not symmetric: both translational and rotational symmetries are broken due to the movement of the molecules. However, one should notice that from the macroscopic point of view this is not the case, because the velocity, temperature and density at a given point are time-independent. Figure 2.7 shows a simulation result of a model introduced by Swift and Hohenberg [1977].

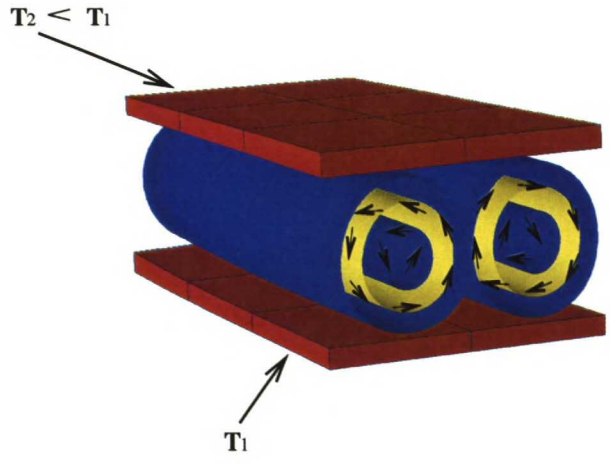

Figure 2.6: The figure shows qualitatively the idea of Rayleigh-Bénard convection. Bénard cells are formed and the fluid starts to move in circular fashion and to opposite directions in neighborhooding cells. The situation shown in the figure is ideal and in reality the cells are not always in parallel and defectless.

Figure 2.7: Computer simulation of Rayleigh-Bénard convection using the Swift-Hohenberg model. The view is from above. Notice that the convective cells are not ordered as in the ideal situation of Figure 2.6. The dark and light colors denote the domains with upward movement (warmer sparse liquid) and downward movement (cooler dense liquid), respectively. The figure is reproduced from [Karttunen, 2001].

Let us now approach the experiment from a more theoretical perspective and determine a control parameter describing the instability. This control parameter is a dimensionless number, which captures the essential features of the system. We will not rigorously derive the Rayleigh number R, i.e., the control parameter of this particular system, but we will take a look at the most important quantities that affect the Rayleigh-Bénard instability and the Rayleigh number.

The thermal expansion discussed above is of course important. As ΔT is small we can approximate change in the density ρ (or mass) using linear response, i.e., $\rho = \rho_0 + \rho\alpha(T_2 - T_1)$, where α is the thermal expansion coefficient. In the analysis, the distance of the plates h, gravitational acceleration g and viscosity of the fluid ν define also characteristics of the system. In addition, by using thermal conductivity k and specific heat C_p of the fluid at constant pressure, we can define thermal diffusivity $\kappa = k/\rho C_p$. With help of these characteristics the Rayleigh number can be derived by dimension analysis, which yields

$$R = \frac{\alpha g \Delta T h^3}{\kappa \nu} \tag{2.3}$$

The Rayleigh number is indeed a dimensionless combination of dimensional parameters. According to Cross and Hohenberg [1993], who offer a very technical approach to this experiment, the instability occurs at $R = 1708$, independent of the fluid.

2.2.3 Turing-type chemical pattern

The experiments discussed above are very important in illustrating the basics of nonlinear dynamics and pattern formation. There exist many different mechanisms for pattern formation and one should not mix the very different underlying physical situations by making conclusions about the qualitative similarity of patterns.

Turing patterns are stationary patterns defined by chemical concentrations and they originate from a coupling of reaction and diffusion processes. Furthermore, Turing systems involve spontaneous symmetry-breaking, i.e., the diffusion acts as a destabilizing force and leads to a bifurcation in proximity of a steady state. In addition, Turing patterns have a characteristic wave length, which depends only on the concentrations, input and output rates, diffusion coefficients and reaction rates of the chemicals. One should notice that the last condition is not fulfilled in the case of Bénard cells, because the size of the cells depends on the geometrical properties

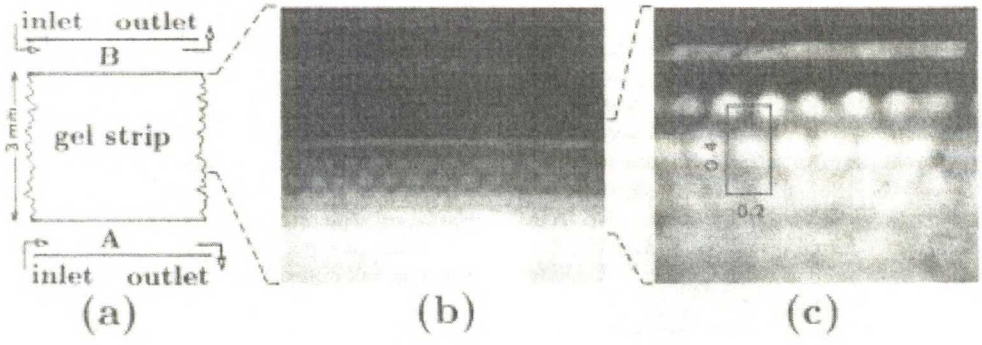

Figure 2.8: Turing-type chemical pattern in a gel strip reactor. The substances A and B diffuse from the reservoirs and react in the gel strip resulting in the pattern seen in b and enlarged in c. The figure is reproduced from Castets et al. [1990].

of the system, i.e., the distance between the planes and not only on the chemical parameters.

The first unambiguous experimental evidence of Turing-type pattern was found by Castets et al. [1990]. Although the article presents strong evidence and agreement with theoretical predictions, the authors used the word "Turing-type" to be careful. The experimental setup is illustrated in Figure 2.8. The gel strip is a transparent chemically inert hydrogel with dimensions $20 \times 3 \times 1$mm. The two long sides of the gel strip are in contact with chemical reservoirs A and B, which are kept at constant concentration. The solutions A and B diffuse from the reservoirs to the gel strip and react together giving rise to a spatial pattern shown in Figure 2.8. The experiment involves a complex chemical treatment of the gel strip and the solution. The typical time to establish a pattern is 3 hours and the pattern may remain unchanged more that 20 hours. These time scales describe well the coarse-grained nature of the theoretical Turing models. Using atomistic simulation methods we could simulate microseconds at best.

Chapter 3

Numerical Approach

In this chapter, the general form of Turing system will be introduced and it will be shown, how the equations are solved in practice. This means applying Euler's method and finite difference method after the problem has been discretized. Both methods are well-known and can be found from any comprehensive numerical analysis book, e.g. [Harris and Stocker, 1998]. This chapter will continue with standard von Neumann stability analysis of the problem. Finally, computational details, visualization and encountered problems will be discussed.

3.1 The general form of Turing system

The general form of Turing system for modeling the evolution of the concentrations of two chemicals, i.e., morphogens is given by two coupled partial differential equations

$$\begin{aligned} u_t &= D_u \nabla^2 u + f(u, v) \\ v_t &= D_v \nabla^2 v + g(u, v), \end{aligned} \tag{3.1}$$

where $u \equiv u(\vec{x}, t)$ and $v \equiv v(\vec{x}, t)$ are the concentrations, and D_u and D_v the respective diffusion constants setting the pace of diffusion. The term ∇^2 denotes the diffusion across the area and the subindex t time derivation, i.e., how fast the concentration varies. The reaction is described by functions f and g that are typically non-linear. The term morphogen was introduced by Turing [1952] to specifically point out the effect of these chemicals on morphogenesis.

The reaction-diffusion mechanism resulting in the instability can be understood with help of the following example, which requires only common sense. Turing discussed the problem of missionaries and cannibals. Think of an island, which is populated by cannibals. Now, missionaries come to the island by boat and want to evangelize the cannibals. If two or more missionaries meet one cannibal they can turn this cannibal into a missionary. If the relative strength is the other way around, the missionaries get killed and eaten by the cannibals. As the missionaries die, more missionaries are brought to the island. In addition, cannibals reproduce with other cannibals.

The concept in the above example is diffusion, i.e., the movement of cannibals and missionaries, which makes the system unstable. This characteristic is called diffusion-driven instability or Turing mechanism. In this example the missionaries have bicycles and they move faster, i.e., they represent the inhibitor of the reaction, i.e., they want to slow down the reproduction of the cannibals, which are in this case the activator. Based on these definitions one can notice the autocatalytic nature of the Turing mechanism: in areas with a lot of cannibals the number of cannibals will increase, because the cannibals will reproduce and more effectively kill the missionaries. On the other hand, the predominance of the cannibals means that more missionaries will be brought to the island to convert them. Finally, the cannibals and missionaries will find a balance. This is a funny example, but it illustrates well the very essence of Turing systems.

3.2 Solving of equations

The problem with a system of partial differential equations of the form of Eq. (3.1) is that typically they cannot be solved analytically, hence numerical methods are needed. We discretize the problem, i.e., transform it from an infinite dimensional to a finite dimensional form. In practice this means that the continuous problem is discarded and a fixed domain of size $M \times N$ (in 2D) is introduced. If we want to solve the problem in three dimensions, the size of the fixed domain is $M \times N \times P$. Here M, N and P stand for the respective lengths of the sides of the simulation domain, i.e., how many grid sites are used in each direction. For simplicity, the equations are usually solved in a rectangular mesh. The words *lattice*, *mesh* and *grid* are used for the discretized domain and the word *site* means one cell of the mesh.

It is a fundamental fact that the problem of Eq. (3.1) is not well-posed without the knowledge of the initial and boundary conditions. In pattern formation simulations initial conditions are usually random perturbations around the steady-state of the system, because if different initial conditions result in patterns that are topologically the same, it proves the robustness of the system. The boundary conditions are often chosen to be periodic in all the coordinate directions of the system. Periodic boundary conditions mean that the opposite boundaries of the simulation domain are actually next to each other, from which it follows that the system acts as if its dimensions were infinite provided that the system is not too small. We may think of the situation as there would be an unlimited amount of simulation domains with their sides coinciding. In the case of a small system periodic boundary conditions may distort the fields inside the system.

For clarity, let us consider the following simple example, where the unit segment of real axis $\Omega = [0, 1]$ is discretized to 10 sites, i.e., we use $M = 10$. This means that the continuous domain Ω is substituted with a set of points, in this case the set being

$$\Sigma = \{0.05, 0.15, 0.25, 0.35, 0.45, 0.55, 0.65, 0.75, 0.85, 0.95\}.$$

Now the periodic boundary conditions would mean that the points 0.05 and 0.95 see each other as neighboring points, e.g. like 0.25 and 0.35. Furthermore, any function value can only have values on the discrete points of set Σ, the values for other points of Ω must be interpolated.

In order to make the numerical process more transparent we will show how the discretization is done and demonstrate the numerical methods in a two-dimensional case. The extension to three dimensions is straightforward and would in this case only make the notations more complicated due to having three-dimensional matrices.

3.2.1 Discretization

A Turing system in two dimensions poses us a problem, where we have to discretize equations of the following form

$$\begin{cases} y_t = D\Delta y + f(x_1, x_2, t) & \text{in } \Omega = [0, L_x] \times [0, L_y] \\ y(x_1, 0, t) = y(x_1, L_y, t) \\ y(0, x_2, t) = y(L_x, x_2, t) \\ y(x_1, x_2, 0) = g(x_1, x_2). \end{cases} \tag{3.2}$$

In the above formulation the topmost equation defines the problem and the domain where has to be solved. The next two equations express the periodic boundary conditions, and the last equation fixes the initial conditions with help of function $g(x_1, x_2)$ defined in the domain. As was mentioned previously, in the case of Turing systems the function g is usually a uniform distribution of random numbers rather than a function in the usual sense.

For simplicity the lattice constant ($dx = h$) is chosen to be isotropic, i.e., $h = h_1 = h_2$. Now the notation y_{ij} is used for the approximation of $y(ih_1, jh_2, t)$, the value of y at the lattice site (i, j) at time t. Using this, we get the matrix

$$y_h(t) = \begin{pmatrix} y_{11} & \dots & y_{1L_y} \\ \vdots & \ddots & \vdots \\ y_{L_x 1} & \dots & y_{L_x L_y} \end{pmatrix}.$$

Next we discretize the function f over the domain matrix by setting

$$f_h(t) = \begin{pmatrix} f(h, h, t) & \dots & f(h, L_y h, t) \\ \vdots & \ddots & \vdots \\ f(L_x h, h, t) & \dots & f(L_x h, L_y h, t) \end{pmatrix}.$$

and the initial conditions analogously

$$g_h(t) = \begin{pmatrix} g(h, h, t) & \dots & g(h, L_y h, t) \\ \vdots & \ddots & \vdots \\ g(L_x h, h, t) & \dots & g(L_x h, L_y h, t) \end{pmatrix}.$$

Using these matrix notations we now proceed and apply some suitable method to solve the partial differential equation.

3.2.2 Euler's method

The Euler's method is well-known citepharris and simple for solving differential equations. The method is based on numerical integration of differential equations. In our case, we use it for the integration over the time step. First, we give a short review of the method itself.

In the general case, Euler's method is used for solving simple first order differential equation of the form $y'(t) = f(t, y(t))$. As the derivative y' is approximated by difference quotient, we obtain the equation

$$\frac{y(t_i + \delta) - y(t_i)}{\delta} \approx f(t_i, y(t_i)) + O(\delta), \tag{3.3}$$

where $O(\delta)$ is an error term of order δ, such that

$$\lim_{\delta \to 0} \frac{O(\delta)}{\delta} = 0.$$

By dropping the error term, Eq. (3.3) can be further reduced to

$$y(t_i + \delta) \approx y(t_i) + f(t_i, y(t_i)) \cdot \delta. \tag{3.4}$$

In our discrete Turing system we fix the time step as δ (or dt). By setting $y_h^k = y_h(k\delta)$, we obtain for Euler's method

$$\begin{cases} y_h^{k+1} = y_h^k + \delta(D\Delta_h y_h^k + f_h^k) \\ y_h^0 = g_h, \end{cases} \tag{3.5}$$

where Δ_h denotes the discretized laplacian, the derivation of which will be presented next.

3.2.3 Finite difference method

The difference method is widely used in problems involving the numerical calculation of the laplacian operator $\nabla^2 = \Delta$. In our two-dimensional study, the laplacian of the function $y(x_1, x_2)$ can be written out as follows

$$\Delta y = \frac{\partial^2 y}{\partial x_1^2} + \frac{\partial^2 y}{\partial x_2^2}. \tag{3.6}$$

In the three-dimensional case, the operator would contain second derivative also in the third direction. By approximating the derivatives twice in the same way as in the previous section and using the notation $y_{i,j}$ for $y(hi, hj)$ we obtain

$$\frac{\partial^2 y}{\partial x_1^2} \approx \frac{y_{i+1,j} - 2y_{i,j} + y_{i-1,j}}{h^2}. \tag{3.7}$$

By repeating the above procedure for derivatives with respect to y, we can write the discretized laplacian operator for Eq. (3.5) as $\Delta_h = I \otimes \Delta_{h_1} + \Delta_{h_2} \otimes I$, where

$$\Delta_{h_p} = \frac{1}{h_p^2} \begin{pmatrix} -2 & 1 & \dots & 0 & 1 \\ 1 & -2 & \dots & 0 & 0 \\ \vdots & \ddots & \ddots & \ddots & \vdots \\ 0 & \dots & 1 & -2 & 1 \\ 1 & \dots & 0 & 1 & -2 \end{pmatrix}.$$

for $p = 1, 2$. Notice that periodic boundary conditions are properly taken into account.

3.3 Fourier transform

Fourier transform is a widely used method for spectral analysis and an introduction to the subject can be found from any basic book handling university level mathematics. The name is to honor a French scientist, Jean-Baptiste Joseph Fourier, a contemporary of Napoleon, who invented the idea of describing a function as a linear combination of other functions. As the Fourier series is extended to continuous case the sum becomes an integral and we can define the one-dimensional Fourier transform $H(\omega)$ of the function $h(t)$ as

$$H(\omega) = \int_{-\infty}^{\infty} h(t) e^{i\omega t} dt, \tag{3.8}$$

and the inverse transform as

$$h(t) = \frac{1}{2\pi} \int_{-\infty}^{\infty} H(\omega) e^{-i\omega t} d\omega, \tag{3.9}$$

where t denotes the time and ω the angular frequency. Here, we want to obtain a three-dimensional transform only with respect to space. This could be thought of in

the following way: t has the unit second s and ω the unit $1/s$. When we transform spatial coordinate $\vec{x}$ which has describes length, e.g. units m, we get something with unit $1/m$. This is of course the wave vector $\vec{k}$. When we write the Fourier transform for our purposes we get

$$H(\vec{k}) = \int_{\Omega} h(\vec{x}) e^{i\vec{k}\cdot\vec{x}} d\vec{x}, \tag{3.10}$$

where Ω denotes the three-dimensional domain and the operator $\cdot$ the scalar product of the two vectors.

3.3.1 Discrete Fourier transform

In our problem, the data is discrete and instead of the continuous transform defined by Eq. (3.10) we have to use discrete Fourier transform (DFT). A brief introduction to DFT can be found from [Press et al., 1995]. The idea is to transform the integration to a sum of discrete values such that the DFT corresponding to Eq. (3.8) is given by

$$H(\omega_n) = \Delta \sum_{j=0}^{N-1} h_j e^{ijn/N}, \tag{3.11}$$

i.e., discrete points h_j of the time domain are transformed to discrete points ω_n of the frequency domain. The calculation of DFT is not straightforward due to its time consuming nature. There are several algorithms for calculating the transform, the most used being the fast Fourier transform (FFT).

3.3.2 FFTW

It is useless to build a code for Fourier transform within the simulation code because there are many libraries developed for this task. Fastest Fourier Transform in the West (FFTW) [Frigo and Johnson, cited 5.12.2001] is a free software developed at the Massachusetts Institute of Technology. It is easy to use and offers both real and complex transforms in one or more dimensions. One of the great features of the libraries is that they adapt to many platforms and can optimize themselves autonomously. In addition, the transform is very fast as the name states.

3.4 von Neumann stability analysis

The von Neumann stability analysis is a method for analyzing stability of a difference equation. A review of the method can be found for example from [Press et al., 1995]. Application of the method on the above problem will be presented next.

The difference equation in three dimensions equation is given by

$$\begin{aligned}\frac{y_{mnp}^{t+1} - y_{mnp}^{t}}{\delta} &= \frac{D}{h^2}(y_{m+1,n,p} + y_{m-1,n,p} + y_{m,n+1,p} + y_{m,n-1,p} + y_{m,n,p+1} + \\ &+ y_{m,n,p-1} - 6y_{mnp}) + f_{mnp}^{t}(y), \end{aligned} \tag{3.12}$$

where h denotes the lattice constant and δ the time step.

Let us now consider that the difference equation varies so slowly that we can try independent solutions of the form

$$y_{m,n,p}^{t} = \xi^t e^{ik_x mh} e^{ik_y nh} e^{ik_z ph}, \tag{3.13}$$

where i is the imaginary unit, and k_x, k_y and k_z the wave numbers in x-, y- and z-directions, respectively. It should be noted that the lattice constant h is the same in all directions as discussed before.

When we substitute Eq. (3.13) to Eq. (3.12) and simplify we get

$$\xi = \frac{D\delta}{h^2}(e^{ik_x h} + e^{-ik_x h} + e^{ik_y h} + e^{-ik_y h} + e^{ik_z h} + e^{-ik_z h} - 6) + 1 + \frac{\delta f_h^t(y)}{\xi^n (e^{mk_x} e^{nk_y} e^{pk_z})^{ih}}, \tag{3.14}$$

We can further approximate $\xi(k)$ by transforming complex numbers to trigonometric functions using Euler's formula and by minoring the cosines with minus one. This yields

$$|\xi(k)| \leq |1 - \frac{12D\delta}{h^2} + \frac{\delta f_h^t(y)}{\xi^n (e^{mk_x} e^{nk_y} e^{pk_z})^{ih}}|. \tag{3.15}$$

We are interested in the modulus of ξ, called the *amplification factor*. Condition $|\xi(k)| < 1$ for all k, implies that the difference equation is stable, i.e., no mode is exponentially growing. The last term on the right side of Eq. (3.15) is dependent on the reaction kinetics of the equation. Thus we handle the general Turing system and the Gray-Scott model separately. Notice that in addition the two equations of each

system must be analyzed separately, because the stability conditions are different. However, δ and h must be chosen equal for both equations of a system due to the coupling of the equations.

3.4.1 General Turing system

It will be shown in Chapter 4 that the kinetics of the general Turing system are given as

$$\begin{aligned} f(u,v) &= \alpha u(1 - r_1 v^2) + v(1 - r_2 u) \\ g(u,v) &= v(\beta + \alpha r_1 uv) + u(r_2 v - \alpha). \end{aligned} \tag{3.16}$$

As we linearize the above equations, we are left with $f(u,v) = \alpha u + v$ and $g(u,v) = \beta v - \alpha u$. To make the approximation reasonable we use the same trial solution for both u and v in the form of Eq. (3.13), except that we make a phase shift of π radians between u and v. This is due to the cross-activator-inhibitor nature of the system.

When we substitute our linearized kinetics to Eq. (3.15) and simplify the equations, we get

$$\begin{aligned} \max|\xi_u(k)| &= |1 - \delta_u(\frac{12D_u}{h^2} - 1 - \alpha)| \\ \max|\xi_v(k)| &= |1 - \delta_v(\frac{12D_v}{h^2} - \beta + \alpha)|. \end{aligned} \tag{3.17}$$

Figure 3.1 shows the plots of Eq. (3.17) for $\max|\xi(\delta)|$, when the lattice constant is fixed to $h = 1$ and parameter values correspond to different modes. The selection of the parameter values will be discussed in more detail in Chapters 4 and 5. For now, the parameter values should be considered just given. The suitable values of δ are the ones where $\max|\xi(\delta)|$ is below the unity, which has been drawn in Figures 3.1 and 3.2 for clarity. Notice that the bottom row of Figure 3.1 implies problems, because with the third set of parameters the first equation for chemical u is not stable for any δ. This can be seen from Figure 3.1e since the amplification factor is larger than one and thus unstable for all values of δ. However, in practise the nonlinear effects and the coupling of the equations stabilize the iteration. Based on this analysis we found that values $h = 1$ and $\delta = 0.05$ were suitable for the general Turing system.

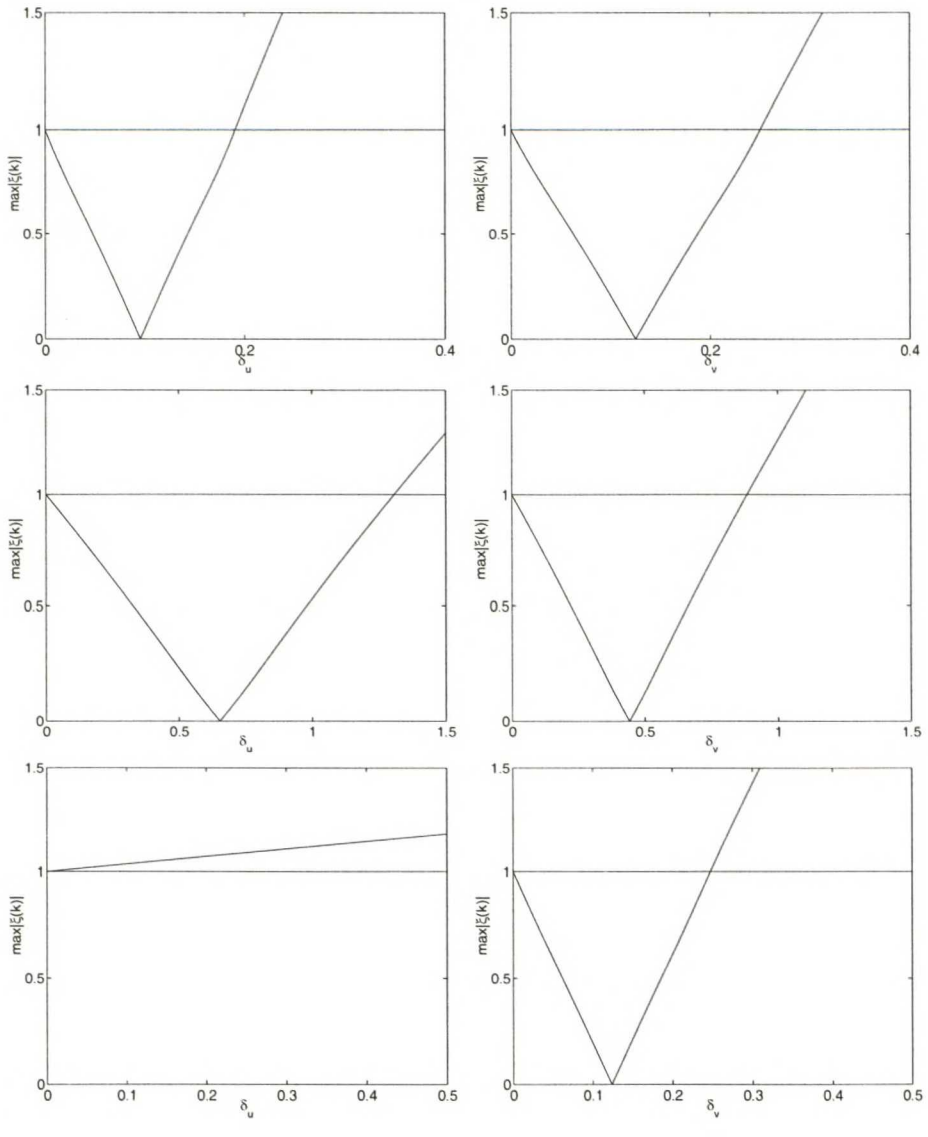

Figure 3.1: Plots of Eq. (3.17) for the used sets of parameters. Figures on the left column (a, c and e) correspond to the equations of u and b, d and f to the equations of v. The parameters of the system were in a and b) $D_u = 1.032$, $D_v = 0.516$, $\alpha = 0.899$ and $\beta = -0.91$, c and d) $D_u = 0.244$, $D_v = 0.122$, $\alpha = 0.398$ and $\beta = -0.4$, e and f) $D_u = 0.129$, $D_v = 0.516$, $\alpha = 0.89$ and $\beta = -0.99$.

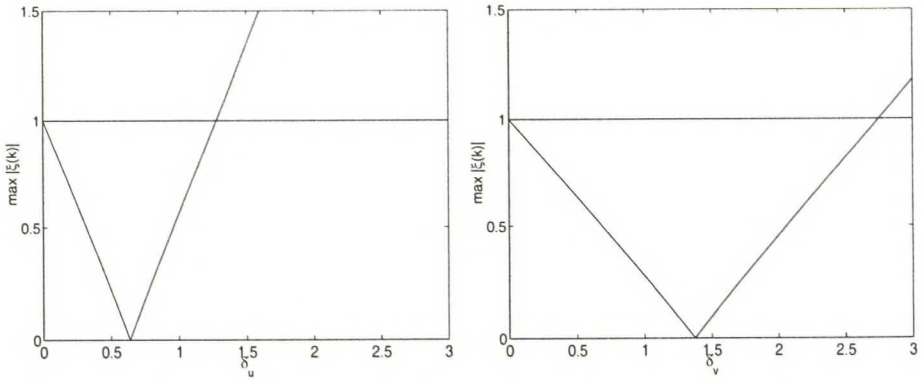

Figure 3.2: Plots of Eq. (3.19) for the used set of parameters. Figure on the left corresponds to the equation with u and the one on the right to the equation with v. The parameters were $D_u = 0.125$, $D_v = 0.05$, $F = 0.045$ and $K = 0.065$.

3.4.2 Gray-Scott model

It will be shown in Chapter 5 that the kinetics of the Gray-Scott model are given as

$$\begin{aligned} f(u,v) &= -uv^2 + F(1-u) \\ g(u,v) &= uv^2 - (F+K)v. \end{aligned} \tag{3.18}$$

When the equations are linearized and the constant term is neglected we are left with $f(u,v) = -Fu$ and $g(u,v) = -(F+K)v$. By following the same procedure as in the previous section, we get

$$\begin{aligned} \max|\xi_u(k)| &= |1 - \delta_u(\frac{12D_u}{h^2} + F)| \\ \max|\xi_v(k)| &= |1 - \delta_v(\frac{12D_v}{h^2} + F + K)|. \end{aligned} \tag{3.19}$$

Figure 3.2 shows the resulting plots for one of the used modes. Based on this analysis and numerical tests we chose values $h = 1$ and $\delta = 1$. Notice that this model allows much bigger time step than the general Turing model.

3.5 Computational details

As one begins to write a simulation program, the following questions in addition to the numerical algorithm selection and analysis should be considered: Which

programming language should be used? How the code can be optimized by programming tricks and using compiler flags? How should the data be read from the program? How can the results be visualized? In this section we concentrate on the first three questions and some other technical details. The last question will be discussed in the next section.

The simulation program was made using C programming language, since it is a simple but versatile language and it is known that C together with Fortran are the most efficient languages for computational tasks. An additional advantage is that MATLAB offers a wide application program interface for both of these languages. The interface can be used to exchange data between MATLAB and the simulation program or to use MATLAB's functions in the program – or vice versa.

Due to the nature of our problem, we chose not to use any algorithm toolboxes and wrote the whole program ourselves. However, for setting the initial conditions we used random number generator RANMAR [Marsaglia and Zaman, 1987], which is considered as one of the best random number generators publicly available. This addition was made only later when we noticed that the generic rand-function of C failed. The old truth is that one should never use the random number generators that come as black boxes.

At first, the simulations were made in two dimensions and the extension to three dimensions was made later. The two-dimensional simulations were made with mesh sizes ranging from 30×30 to 1000×1000. Adding the third dimension led to significant changes, since a three-dimensional system of size $100 \times 100 \times 100$ has as many lattice sites as a two-dimensional system of 1000×1000. In addition, the simulation is slower, because in three dimensions the laplacian must always be calculated to six directions compared as to four. To make simulation time reasonable we used a system of $50 \times 50 \times 50$. The number of time steps taken was usually $10^4 - 10^6$.

In our program there were not many things to be optimized. However, the use of memory and the number of for-loops were decreased to minimum. With this kind of systems one should be careful with the allocation of memory for arrays. If you are not, you might suddenly have ten or more $50 \times 50 \times 50$ arrays, each holding 125000 8 byte doubles, which is often useless. The calculation of laplacian was optimized in the following way: First the differences were calculated for the sites that were not on the boundary. Only after that the differences were calculated for the boundary

sites. This was beneficial since otherwise we would have had to check inside a triple for-loop whether a site is on the boundary or not.

The convergence of the iterations was checked by observing the change in the values of each site. When this quantity was on average $\backsim 10^{-6}$ the system was considered to be stable enough and the simulation was stopped. It should be noted that due to the nature of the system, it approaches the final state asymptotically, never completely reaching it. Another problem is that the system may become locked in a meta-stable state for a very long time thus making the system seemingly stable. When this was suspected, simulations with millions of time steps were ran. Another way to get the system out of meta-stable states is to add random noise. This will be discussed in Chapter 4.

The calculation of structure factors was made computationally lighter and more precise by changing the intuitive order of the procedures: we did not transform the pair correlation function but we calculated the Fourier transform of the data and defined the structure factor from it.

For visualization and analysis the data was read from the program using MX- and MAT-routines of MATLAB for file and memory management, which resulted in the dependence on MATLAB libraries. Thus the code is not easily portable between platforms, which is not desirable, but in this case necessary. We tried also to write the data in ASCII form, but this resulted in big text files and slow data reading. All these problems were caused by a bigger problem, which we will turn to next.

3.6 Visualization

Every time a researcher makes simulations, he or she faces the same problem: Suitable tools for visualizing the data should be found. There are many programs for visualizing different kind of data. Generally speaking, the most used is MATLAB due to its easy-to-use environment and functions. The visualization of our two-dimensional studies was made with MATLAB. We had a two-dimensional array designating concentration values for each site of the mesh. Hence our data was actually three-dimensional – two position coordinates and a data value. This kind of data can be simply visualized by a surface or a contour plot for which MATLAB offers suitable tools.

The visualization of the three-dimensional Turing system made everything much more complicated. In this case the data is actually four-dimensional having three position coordinates and a data value. With MATLAB one could only do simple slicing the data but this was not sufficient in this case due to the data being continuous and very complex. The answer to the problem was FUNCS, a Finnish visualization software developed by the Centre for Scientific Computing.

FUNCS is for visualization and animation of multi-channeled two- or three-dimensional data on Silicon Graphics (SGI) computers. The user may set the color and transparency for each data value. Using volume shading, FUNCS gives a picture that can be rotated and zoomed. For simplicity, we discretized the data to zeros and ones, where zero indicates that the dominating chemical on the site is u and one indicates v. Thus the resulting picture has only two colors. Blue color was used for the concentration of chemical v and yellow for chemical u. To make the picture clearer, yellow was set to be transparent. This simplification was possible since the Turing systems are usually cross-activator-inhibitor systems, meaning that only one chemical dominates in certain domain, and, in addition, the interfaces of these domains are sharp.

The dependence on MATLAB due to the data being imported to FUNCS as raw SGI-binary, which is written with the help of MATLAB. Another possibility would be running the simulation program only in SGI computers and write SGI-binary directly. However, this line of thought was not pursued.

The other visualization software that was used, was an open source software called OpenDX developed by IBM. OpenDX enables the real-time visualization of the simulation using a sophisticated data transfer methods between two computers, i.e., we simulate the system using a fast processor or many processors and the data is sent out almost continuously to the visualization program which does not have to be ran on the same computer as the simulation. In this way, it is straightforward to make movies showing the development of the morphology. For discussion about the advantages and disadvantages of OpenDX, and details of the client-server approach see [Mustonen, 2001]. However, no matter how sophisticated the visualization software is, the problem remains that one cannot really see inside a three-dimensional object.

Chapter 4

General Turing System

This chapter concentrates on building, analysis and numerical simulation of a general of Turing system. This model is called general due to the nature of the reaction kinetics, which make it possible to study the effect of different couplings and nonlinear terms. The model was introduced in [Barrio et al., 1998]. We use linear analysis to predict the behavior of the system, and the numerical methods presented in the previous chapter for solving the system using computer simulation. Finally, the results are presented and analyzed with the help of structure factors.

4.1 The model

First, we consider the general form of a Turing system that was already introduced in the beginning of Chapter 3. It is given for two chemicals U and V as

$$\begin{aligned} U_t &= D_U \nabla^2 U + f(U,V) \\ V_t &= D_V \nabla^2 V + g(U,V), \end{aligned} \tag{4.1}$$

where $U \equiv U(\vec{x},t)$ and $V \equiv V(\vec{x},t)$ are the spatially and temporally varying concentrations.

This system has a steady-state (U_c, V_c) defined by $f(U_c, V_c) = g(U_c, V_c) = 0$. The equations of motion are obtained by phenomenological expansion of the nonlinear reaction functions f and g around the stationary uniform solution (U_c, V_c). Keeping

terms up to cubic order, we get for the reaction terms

$$f(U,V) = A(U-U_c) + B(V-V_c) - C(U-U_c)(V-V_c) - D(U-U_c)(V-V_c)^2$$
$$g(U,V) = E(U-U_c) + F(V-V_c) + C(U-U_c)(V-V_c) + D(U-U_c)(V-V_c)^2,$$

where A, B, C, D, E, F are constants to be determined. Notice that the coefficients of the nonlinear terms must be chosen to be opposite numbers due to the cross-inhibitor-activator nature of the system. Fixing $B = 1$ and denoting $A = \alpha$, $C = r_2$, $D = \alpha r_1$, $E = \gamma$, $F = \beta$ yields

$$\begin{aligned} u_t &= D\delta\nabla^2 u + \alpha u(1 - r_1 v^2) + v(1 - r_2 u) \\ v_t &= \delta\nabla^2 v + v(\beta + \alpha r_1 uv) + u(\gamma + r_2 v), \end{aligned} \tag{4.2}$$

where $u = U - U_c$ and $v = V - V_c$, making the point $(u, v) = (0, 0)$ a stationary solution. The diffusion constant is divided so that δ is a scaling factor and D is the ratio between the diffusion constants of the two chemicals. It is important to notice that $D \neq 1$ is required for the diffusion-driven instability to occur. We consider u to be the activator and v to be the inhibitor chemical, and thus require $D < 1$. The parameters r_1 and r_2 can be used for adjusting the non-linear interactions, and α, β, γ, δ and D for mode selection, which will be discussed in the next section.

The coefficients r_1 and r_2 set the amplitudes of the nonlinear terms, which are crucial for the morphology. It has been pointed out by Barrio et al. [1998] that in two dimensions quadratic interactions (uv) correspond to spot patterns, whereas cubic interactions (uv^2) correspond to stripe patterns. By tuning r_1 and r_2 one can select either one of the interactions or generate a competition between the two patterns by setting both terms nonzero.

4.2 Linear analysis

Linear analysis is a method for studying the stability of a system around a steady-state. By linear analysis we try to find modes, i.e., wave vectors that grow exponentially thus resulting in an instability and complex pattern formation. In addition, we try to choose the parameters in such a way that only certain desired modes will grow. For an introduction to the method see [Nicolis, 1995] or [Murray, 1993].

It has been pointed out earlier [Barrio et al., 1998] in relation to the studies of

two- dimensional Turing systems, that there may exist a number of different modes having the same wave number. This phenomenon is called *degeneracy*. To make the concept conceivable consider two two-dimensional vectors $\vec{k}_1 = (1, 0)$ and $\vec{k}_2 = (0, 1)$. Even though these vectors point to different directions their length is the same $|\vec{k}_1| = |\vec{k}_2| = 1$. In three dimensions the degeneracy is greater and occurs already at small wave numbers. Consider for example vectors $(7, 1, 0), (5, 0, 5), (3, 4, 5)$ and all other possible permutations having the same length $5\sqrt{2}$. Thus the question of which mode will dominate the evolution becomes more difficult to answer in three dimensions.

The above becomes obvious when one recalls that in a finite grid the admissible modes are not continuous but discrete and the modulus of the wave vector is given as

$$|\vec{k}| = k = 2\pi\sqrt{\left(\frac{n_x}{L_x}\right)^2 + \left(\frac{n_y}{L_y}\right)^2 + \left(\frac{n_z}{L_z}\right)^2}, \tag{4.3}$$

where L_x, L_y and L_z denote the system size in respective directions and n_x, n_y and n_z the respective wave number indices. Then the linear analysis proceeds as follows.

As was mentioned earlier, Eq. (4.2) has an stationary solution defined by the zeros of f and g evaluated at steady-state solution $(u, v) = (0, 0)$. By solving the equations

$$\begin{aligned} \alpha u(1 - r_1 v^2) + v(1 - r_2 u) &= 0 \\ v(\beta + \alpha r_1 uv) + u(\gamma + r_2 v) &= 0, \end{aligned} \tag{4.4}$$

we obtain another steady-state solution at

$$v = \frac{-(\alpha + \gamma)}{1 + \beta} u. \tag{4.5}$$

In order to facilitate the analysis, we enforce $(0, 0)$ to be the only stationary uniform solution by setting $\alpha = -\gamma$, thus making the relation of Eq. (4.5) obsolete.

Dispersion relation is an important concept relating to linear analysis. It yields the eigenvalues of the linearized equations as a function of wave number. In the absence of diffusion the linearized system is given as

$$\begin{pmatrix} u_t \\ v_t \end{pmatrix} = \begin{pmatrix} f_u & f_v \\ g_u & g_v \end{pmatrix}_{u_c, v_c} \begin{pmatrix} u \\ v \end{pmatrix}.$$

where the sub-indeces stand for partial derivation and these derivatives are evaluated at the steady state $(u_c, v_c) = (0, 0)$. In the presence of diffusion with the partial derivatives of the reaction kinetics calculated we obtain

$$\begin{pmatrix} u_t \\ v_t \end{pmatrix} = \begin{pmatrix} \delta D & 0 \\ 0 & \delta \end{pmatrix} \begin{pmatrix} \Delta u \\ \Delta v \end{pmatrix} + \begin{pmatrix} \alpha & 1 \\ \gamma & \beta \end{pmatrix} \begin{pmatrix} u \\ v \end{pmatrix}.$$

Now, let $u_k(\vec{r}, t)$ and $v_k(\vec{r}, t)$ be the eigenfunctions corresponding to the wave number k and each function satisfying the boundary conditions. We seek for solutions of form

$$u(\vec{r}, t) = \sum_k c_k e^{\lambda t} u_k(\vec{r}, t) \tag{4.6}$$

$$v(\vec{r}, t) = \sum_k c_k e^{\lambda t} v_k(\vec{r}, t), \tag{4.7}$$

where the constants c_k are determined by the initial conditions. When these solutions are substituted to Eq. (4.2), we obtain

$$\begin{pmatrix} \lambda u_k \\ \lambda v_k \end{pmatrix} = \begin{pmatrix} \delta D & 0 \\ 0 & \delta \end{pmatrix} \begin{pmatrix} -k^2 u_k \\ -k^2 v_k \end{pmatrix} + \begin{pmatrix} \alpha & 1 \\ \gamma & \beta \end{pmatrix} \begin{pmatrix} u_k \\ v_k \end{pmatrix}.$$

The eigenvalues λ are determined by the characteristic polynomial

$$|\lambda I - A + Dk^2| = 0, \tag{4.8}$$

where I denotes the identity matrix, A the linearized matrix and D the matrix with the diffusion constants. Calculation of the determinant yields

$$\lambda^2 - (\alpha + \beta - \delta k^2(1 + D))\lambda + (\alpha - \delta D k^2)(\beta - \delta k^2) + \alpha = 0, \tag{4.9}$$

where $k^2 = \vec{k} \cdot \vec{k}$.

The conditions for diffusion-driven instability to occur are widely known [Murray, 1993] to be the following

$$f_u + g_v < 0 \tag{4.10}$$

$$f_u g_v - f_v g_u > 0 \tag{4.11}$$

$$D_u g_u + D_v f_u > 0 \tag{4.12}$$

$$D_u g_u + D_v f_u > 2\sqrt{D_u D_v (f_u g_v - f_v g_u)}, \tag{4.13}$$

where the partial derivatives are calculated at (u_c, v_c) and $D_u = \delta D$ and $D_v = \delta$ are the diffusion coefficients for chemicals u and v, respectively.

From the above conditions we can conclude that the onset of instability is subject to the following conditions: if $\alpha \geq 0$, then

$$-1 < \beta < -\alpha \tag{4.14}$$

$$\alpha - 2\sqrt{\alpha D} > \beta D, \tag{4.15}$$

and if $\alpha < 0$, then

$$\beta < \min\{-1, -\alpha\} \tag{4.16}$$

$$\alpha - 2\sqrt{\alpha D} > \beta D \ (\alpha > \beta D) \tag{4.17}$$

$$\alpha + 2\sqrt{\alpha D} > \beta D \ (\alpha < \beta D). \tag{4.18}$$

By restricting the parameter selection such that $\alpha \in (0, 1)$ and $\beta \in (-1, 0)$ we are left with only two conditions

$$\beta < -\alpha \tag{4.19}$$

$$\alpha - 2\sqrt{\alpha D} > \beta D. \tag{4.20}$$

The dispersion relation $\lambda(k)$ can be plotted by using Eq. (4.9). The objective is to find parameter values that can be used to isolate modes. Figure 4.1 shows the real parts of the eigenvalues plotted against the wave number k for three modes. In addition, we used an equation for the critical wave number, i.e., the wave number at the maximum of the curve. This is given by

$$k_c^2 = \frac{D(\alpha - \beta) - (D+1)\sqrt{\alpha D}}{\delta D(D-1)}. \tag{4.21}$$

It is worth noticing that the algebraic form of Eq. (4.9) makes it difficult to analyze the system further. This is why Eq. (4.21) is very useful.

4.3 Simulation results

This section presents the results of the three-dimensional simulations. Despite the fact that the structures appear impressive, we cannot draw plausible conclusions

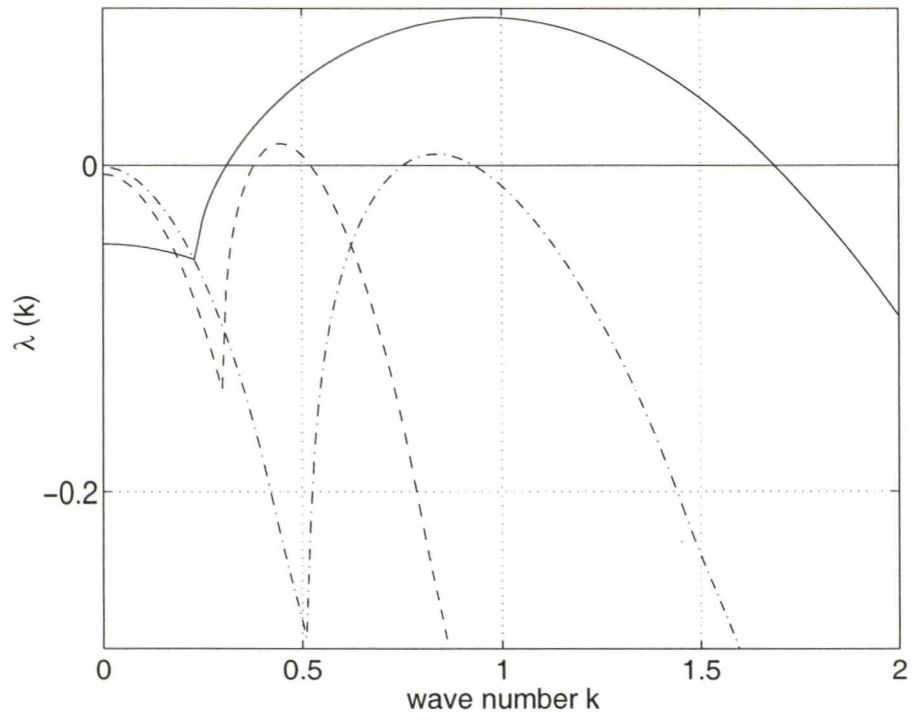

Figure 4.1: The dispersion relation of Eq. (4.2) for selected modes. The parameters were $D = 0.516$, $\alpha = 0.899$, $\beta = -0.91$ and $\delta = 2$ for $k = 0.45$ (dash-dot line), $D = 0.122$, $\alpha = 0.398$, $\beta = -0.4$ and $\delta = 2$ for $k = 0.84$ (dotted line), $D = 0.516$, $\alpha = 0.89$, $\beta = -0.99$ and $\delta = .25$ for $k = 0.96$ (solid line). The region above $\lambda(k) = 0$ bounds the wave number values for unstable modes.

based on a qualitative analysis, although this is probably the best way to analyze the results. Anyway, we try quantitative analysis by determining the structure factors of the structures.

In the following, when we discuss about the additive noise, we mean Gaussian uncorrelated noise which has been added to every site at every time step. On the other hand, by fluctuations we mean perturbations that are added to the final structure to observe its stability. The first and second moments of the noise are given by $\langle \eta(\vec{x}, t) \rangle = 0$ and $\langle \eta(\vec{x}, t)\eta(\vec{x}', t') \rangle = 2\varepsilon\delta(\vec{x} - \vec{x}')\delta(t - t')$. The angular brackets denote an average and ε is the intensity of the noise.

4.3.1 Common structures

First, we compare the behavior of the system in three dimensions to results obtained from a simple two-dimensional simulation [Barrio et al., 1998]. Figure 4.2 shows the reproduced results in two dimensions. In the top row, the parameters were chosen to favor striped patterns, i.e., $r_2 = 0$ and in the bottom row spotty patterns, i.e., the term r_2 was set dominant. Figure 4.3 shows with the same layout as Figure 4.2 the corresponding structures obtained from the simulations of the three-dimensional system.

As can be noticed from the top row of Figure 4.2 there are only a few defects, i.e., points where the stripes coincide. However, in Figures 4.3a and b showing the lamellar structures, a greater number of defects than in the striped two-dimensional patterns can be seen. This is due to the difficulty of aligning planes compared to stripes in parallel. The droplet patterns in the bottom row of Figure 4.2 and structures in Figures 4.3c and d are more similar despite the increase in the dimensionality of the system. However, it can be seen that whereas the two-dimensional system stabilizes to a hexagonal lattice, this kind of pure structure cannot be observed in three dimensions due to the increased number of degrees of freedom. In the next section we will discuss how to obtain regular structures.

Notice that the two modes $k = 0.45$ and $k = 0.84$ differ qualitatively by the wavelength $\lambda = 2\pi/k$. As k increases, the wavelength decreases resulting in patterns with less distance between stripes and larger number of the stripes. In two dimensions the same effect could be also obtained by changing the scaling factor δ in both equations. However, in three dimensions the qualitative difference of the two quan-

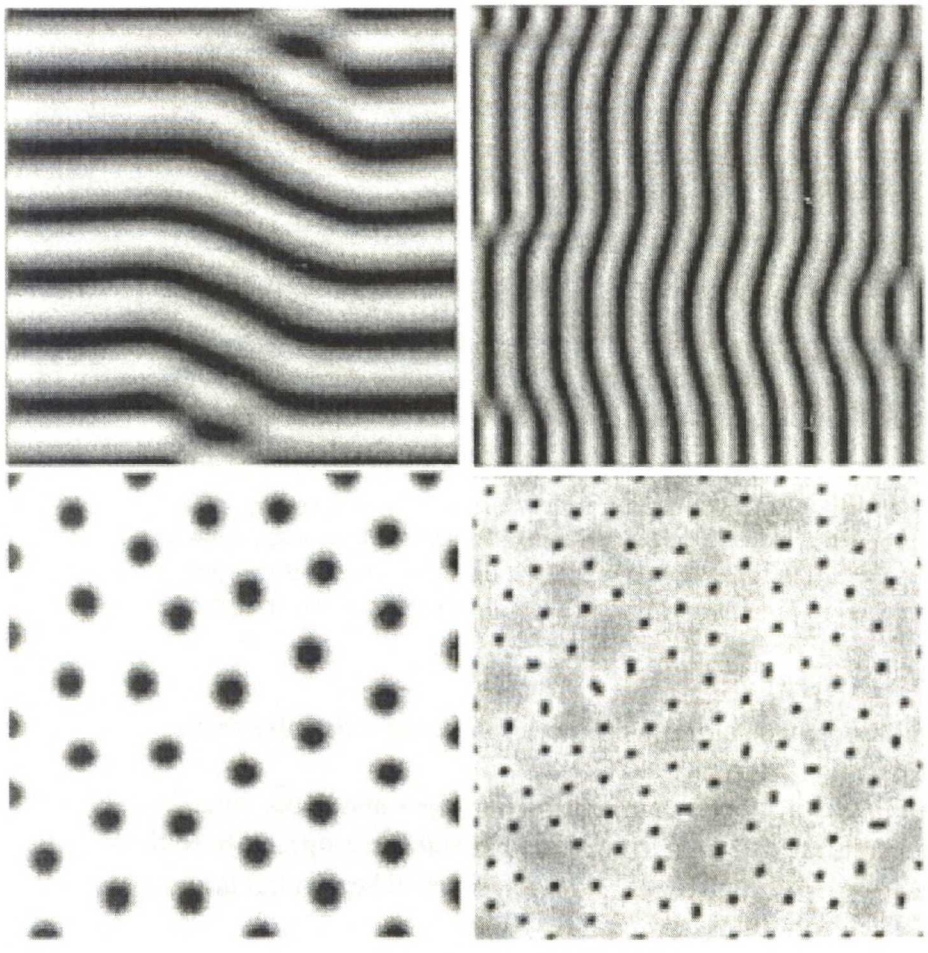

Figure 4.2: Patterns obtained from simulations of the general Turing model in two dimensions using random initial conditions. Top row: $r_1 = 3.5$ and $r_2 = 0$; bottom row: $r_1 = 0.02$ and $r_2 = 0.2$. In the left column, the parameters were chosen to favor $k = 0.45$; in the right column to favor mode $k = 0.84$. Reproduced from [Barrio et al., 1998].

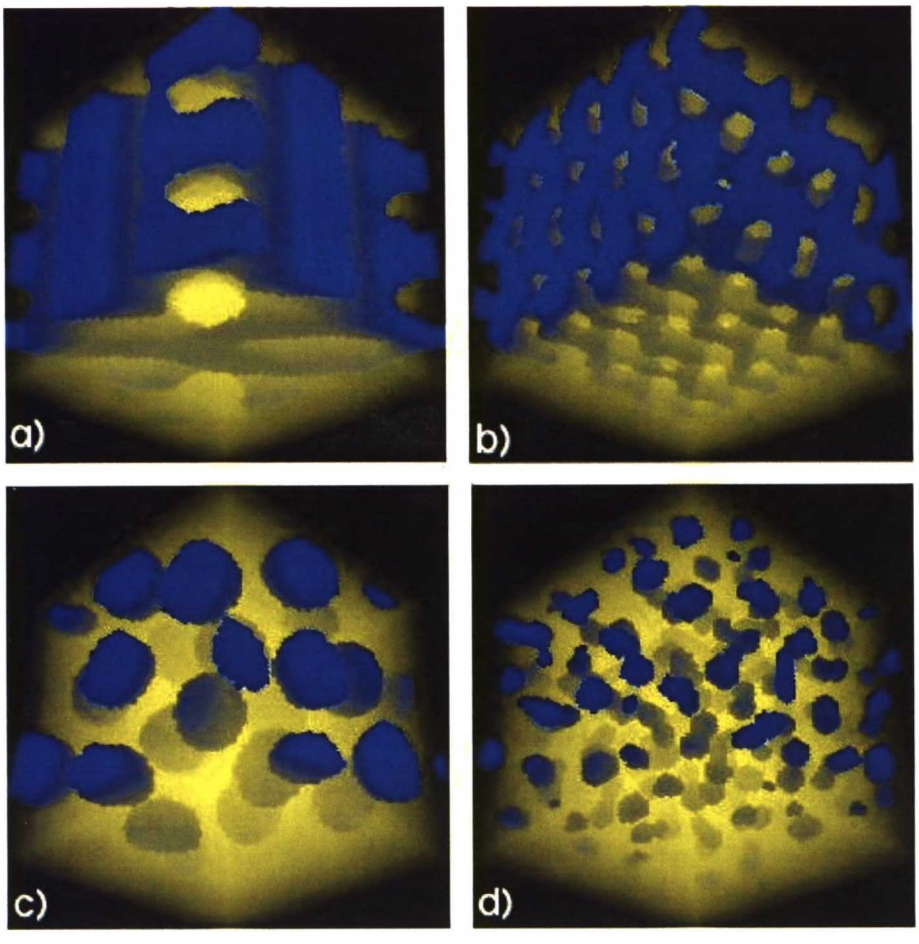

Figure 4.3: Patterns obtained from simulations of the general Turing model after 500 000 iterations and using random initial conditions on every site of the lattice: $u_0, v_0 \in (0, 1)$. Top row: $r_1 = 3.5$ and $r_2 = 0$; bottom row: $r_1 = 0.02$ and $r_2 = 0.2$. Left column, the parameters were chosen to favor $k = 0.45$; in right column to favor mode $k = 0.84$. Compare the results with the two-dimensional patterns in Figure 4.2.

titatively different cases is clearer (Figures 4.3a and b), since while a line has only the slope determining the direction, a plane has two variables aligning it.

The change in the wavelength has the same effect in the case of droplet patterns. The droplets become smaller and the distance between them shorter. It has been pointed out by Barrio et al. [1998] that in two dimensions the spots are more robust than stripes. The robustness means the stability of the pattern or structure with respect to perturbations, different initial conditions or other changes in the simulation conditions. The robustness can be studied e.g. by adding noise. This will be discussed later. As one would expect, the spots turned out to be more robust also in three dimensions. This can be expected based on the fact that the

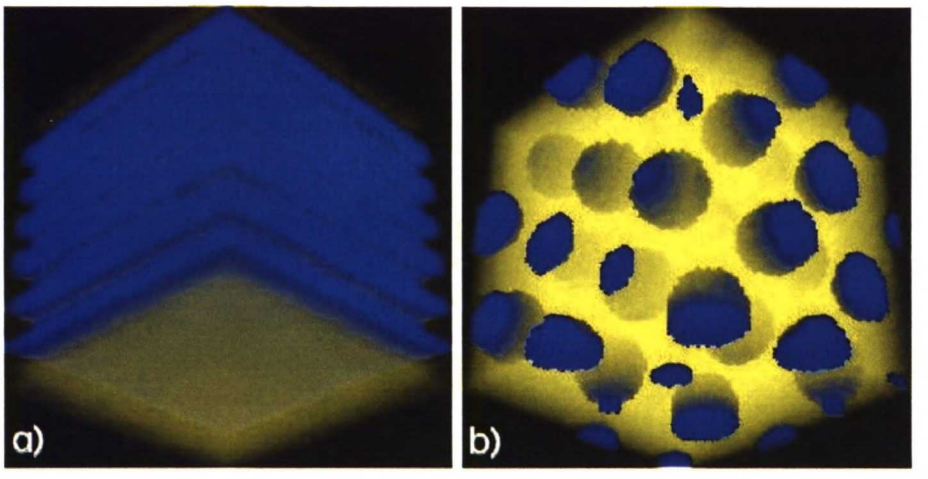

Figure 4.4: Patterns obtained simulation of the general Turing model after 500 000 iterations. Left: Initial conditions: chemical U set in mid-plane, b) initial conditions: chemical U placed on 111-plane in an triangular mesh.

4.3.2 Regular structures

In order to study whether it is possible to obtain pure or single modes, we set up the system such that the initial conditions should favor only one selected mode. Figure 4.4a shows a situation where the system was prepared in such a way that a layer of chemical U was set only in the mid-plane of the simulation box to provide favorable initial conditions for the lamellar structure to develop. The parameters are the same as used in Figure 4.3b. In Figure 4.4b chemical U was introduced only in locations corresponding to 111-plane in an triangular mesh, i.e., favoring hexagonal symmetry of the droplets obtained as in Figure 4.3c. In both cases chemical V was introduced uniformly over the cube as in Figure 4.3. Actually it did not affect the topology of the resulting structures, which one of the morphogens was introduced asymmetrically. The stability of these patterns was also tested against Gaussian noise and both of them turned out to be robust.

Figure 4.5 shows a simulation result corresponding to Figure 4.4a as additive Gaussian noise was used in the way described in the beginning of this section. One can observe that using the initial conditions in the midplane we drive the system robustly to the lamellar structures. Even a substantial amount of noise did not break down the planes, but made them align differently and curve. The spherical droplet structures were much more stable against additive noise, and adding noise did not affect them in any noticeable way. This is due to the amplitude of the unstable wave vectors as was discussed in Chapter 2. Robustness of the model is very important,

Figure 4.5: Results of the simulation which was initialized in the same manner as Fig. 4.4a, but additive Gaussian random noise was used. The noise results in curved and strangely aligned planes.

since when the models are used for studies of biological systems, we have to take into account noise and other disturbing factors that exist in the nature.

4.3.3 Complex structures

Next we want to explore the effect of multiple modes to the morphology of the system. We did this by tuning the parameters in such a way that mode $k = 0.96$ was the most unstable one. In the simulations we used parameters $\alpha = 0.89$, $\beta = -0.99$, $\delta = 0.25$, $D = 0.516$. The nonlinear parameters were $r_1 = 0.02$ and $r_2 = 0.2$ corresponding to droplet patterns. Notice that now the dispersion relation (Figure 4.1) allows many modes to grow (there is a long segment on the k-axis for unstable eigenvalues λ), and this causes rigorous competition and almost chaotic morphology. Figure 4.6a shows the stabilized configuration where the pattern shows a tubular-like structure.

In order to observe the competition between spherical and lamellar structures, we isolated mode $k = 0.45$ and set both r_1 and r_2 different from zero. Using non-linear parameters $r_1 = 3.5$ and $r_2 = 0.2$ resulted in the competition between cubic and quadratic terms favoring lamellar and spherical structures, respectively. The result of this competition can be seen in Figure 4.6b, where one can clearly find round lamellar structures with spherical holes. In this case, it took 2 000 000 time steps to stabilize the structure.

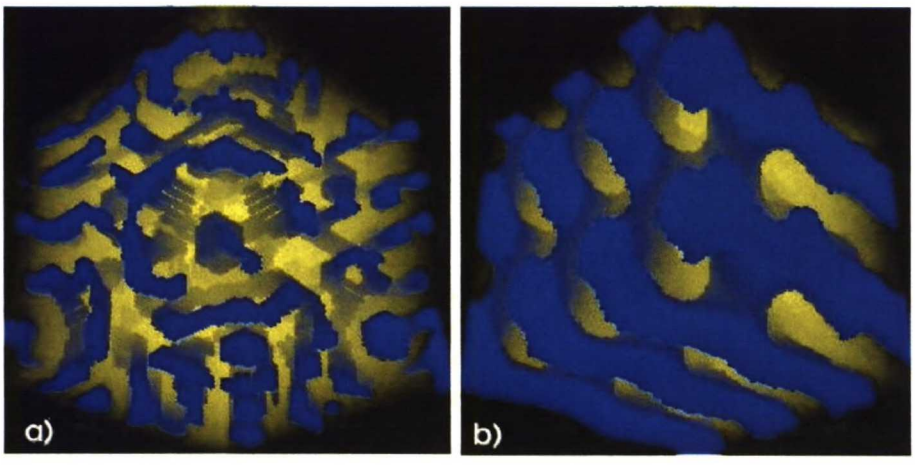

Figure 4.6: Patterns obtained using the general Turing system. a) After 500 000 time steps, the isolated mode was $k = 0.96$ and non-linear parameters $r_1 = 0.02$ and $r_2 = 0.2$, and b) after 2 000 000 time steps, $k = 0.45$, $r_1 = 3.5$ and $r_2 = 0.2$.

4.3.4 The effect of the size of the domain

In the context of mathematical biology it is of great interest to study different kind of growth models, because Turing originally developed the reaction-diffusion system to model morphogenesis. Development and simulation of any real morphogenetic model is beyond the scope of our current work, but these issues will be considered in the future studies.

Due to the unique nature of our three-dimensional simulations, we consider only a simple statically grown system by increasing one dimension of the simulation box between simulations. We will present the Turing system of size $50 \times 50 \times L$ where $L = 2, 4, 8, 16, 32, 64$. Dynamic growth, where the growth factor is added continuously to the system parameters (e.g. [Sekimura et al., 2000]) was considered, but the idea was discarded since we do not yet have enough knowledge about the dynamics of the system to make any plausible conclusions. For simplicity we used zero-flux boundary conditions to all directions. However, we do not believe that this has any significant effect on the topology of the system.

Figure 4.7 shows the preliminary results, when the system is grown statically. The initial conditions are random (the same in all simulations of course) and the parameters are the same as in Fig. 4.3a. The first figure of the system $50 \times 50 \times 2$ is essentially two-dimensional. The most interesting phenomena happens between the systems sized $50 \times 50 \times 4$ and $50 \times 50 \times 8$. The former appears to be nearly two-

third dimension does not bring as much new to the spotty structures as it does to the lamellar structures.

The figures imply that starting from completely random initial conditions, it is not likely for the system to converge into a purely lamellar state. This was confirmed by a number of extensive simulation runs. To make it clear, notice that the difference between Figure 4.3a and b is that the parameters α and β have been selected in such a way as to enhance modes $k = 0.45$ and $k = 0.84$. These are the most unstable modes in the sense of the linear approximation for parameter sets $\alpha = 0.899$, $\beta = -0.91$, $\delta = 2$, $D = 0.516$, and $\alpha = 0.398$, $\beta = -0.40$, $\delta = 2$, and $D = 0.122$, respectively. These particular choices of parameters were made in order to facilitate the comparison with the 2D results. The reason for these choices is that in the first case, in the sense of the linear analysis, there are very few admissible modes with positive growth rates and zero wavenumber degeneracy. As it is clear from Eq. (4.3), degeneracy becomes increasingly important at higher wave numbers. Ideally, the choice $k = 0.45$ should produce patterns with wave vector $\vec{k} = 2\pi(n_x/L, 0/L, 0/L)$, i.e., favoring strongly the lamellar phase when $r_2 = 0$. However, as seen in Figure 4.3a, the system has not reached a lamellar state even after 500 000 time steps but it has converged to a mixed state instead. The simulations confirmed that to be the stable final state.

Figure 4.3b displays the situation where the mode $k = 0.84$ is favored. In this case, there are more closely spaced admissible modes leading to a competition between them. It is important to notice that the system has a finite size and thus there are, in the sense of the linear analysis, only certain admissible modes (Eq. (4.3)). From the topmost figures of Figure 4.3 it is clear that the competition between the modes in the three-dimensional Turing system can lead to very interesting morphologies. The defects in two dimensions can be considered as reminiscents of the more complicated pattern selection in 3D since the 2D stripe patterns can be seen as cuts from a 3D system. However, as seen in Figures 4.3a and b, the 3D case displays much richer behavior and it is very difficult to obtain a purely lamellar pattern starting from random initial conditions.

In the bottom row of Figure 4.3, the parameters r_1 and r_2 have been selected to favor spots, or spherical droplet shapes (these can be compared directly to Figures 2e and 2f in [Barrio et al., 1998]). The droplet patterns turned out to be very robust. In the simulations, these morphologies developed very fast and were also stable against random Gaussian fluctuations that were used to test the stability of the patterns against perturbations as discussed earlier.

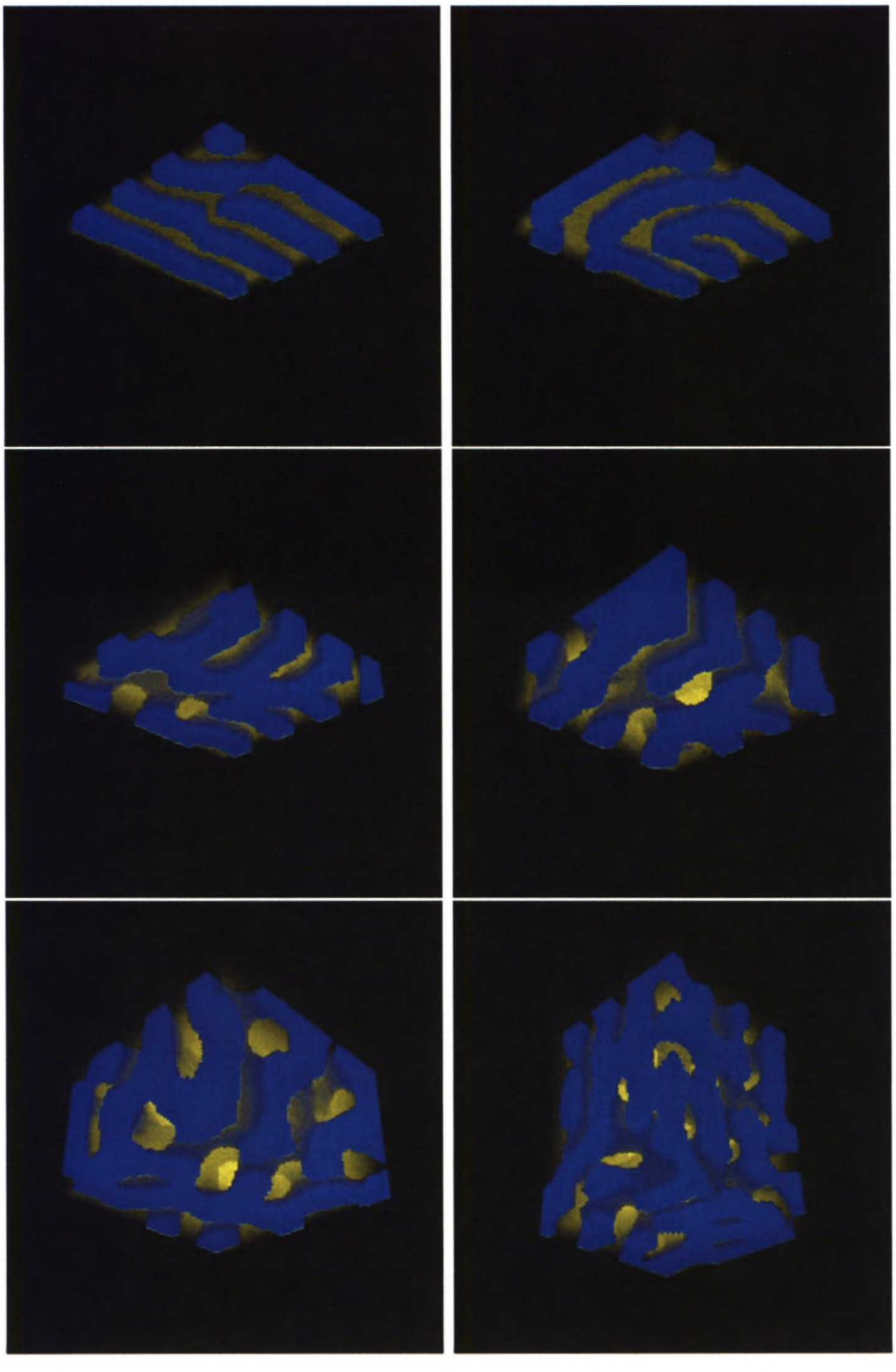

Figure 4.7: The statically growing domain $50 \times 50 \times L$, where on the top row L=2,4, middle L=8,16, bottom L=32,64. All the conditions are the same as in Figure 4.3a.

dimensional (all layers have the same morphology), but the latter shows clearly three-dimensional character (there are vertical holes in the lamellar structures). Based on visual analysis one could conclude that the transition between the second and the third dimension takes place immediately when the shortest dimension of the system is more than the characteristic wave length of the eigenmode.

4.4 Structure factors

In addition to qualitative considerations, it is crucial to introduce some quantitative techniques to analyze the morphologies of the concentration fields or structures obtained by simulations. Although usually very helpful and informative, qualitative analysis can sometimes lead to false conclusion.

In solid state physics the structure factor is commonly used to describe material properties in diffraction, e.g. Bragg diffraction as discussed in [Ashcroft and Mermin, 1976]. According to the Braggs' idea of constructive and destructive interference of scattered X-rays, certain characteristics of the structure can be concluded based on the distribution of X-rays. In practice, the calculation of a structure factor means the Fourier transform of pair correlation function. To confirm the plausibility of the analysis a brief introduction to the concepts mentioned above will be given next.

Consider two parallel planes with distance d between the planes. If two X-rays come in an angle θ and the first ray scatters from the upper plane and the other ray from the lower plane, the well-known Bragg condition for constructive interference of these rays is $n\lambda = 2d\sin\theta$. This formula indicates that the difference between the lengths of the paths taken by the two rays must be an integer multiple (n) of the wave length. For this simple but remarkable idea, father and son, W.H. and W.L. Bragg were awarded a Nobel price in 1915.

One commonly used quantity to describe the regularity of material structure is the pair correlation function, which is a one-dimensional scalar function $g(r)$ defined by the average number of atoms on specific distance from given atom. In other words, there are on average n atoms at distance r_0 from a selected atom. The Fourier transform of the pair correlation function is the structure factor, defined as

$$S(k,t) = \int_0^\infty g(r,t)e^{ikr}dr, \tag{4.22}$$

where the time dependence is introduced to keep the treatment general.

In the current case we do not have atoms but a uniform scalar field defined over the domain. This kind of problem has been handled before, for example in the case of a phase field model [Karttunen et al., 1997], and we follow that procedure. In this case, the structure factor is defined with help of the one- and two-point correlation functions as

$$S(\vec{k},t) = \int_0^\infty (C_2(\vec{x},t;x\vec{+}r,t) - C_1^2(\vec{x},t))e^{i\vec{k}\cdot\vec{r}}d\vec{r}, \tag{4.23}$$

which is just a complex way of saying that we Fourier transform the field after we have subtracted the average from it. The Fourier transform is equivalent to the X-ray diffraction and transforms the data from the real space to the wave vector space. Typically, the structure factor is not examined with respect to wave vector $\vec{k}$, but wave number k. One could also study time development of $S(\vec{k},t)$ by fixing $|\vec{k}|$ and observing the magnitude with respect to time t. The time development is not studied in this thesis.

Using the methods discussed in Chapter 3, we have calculated the structure factors of three qualitatively different structures, and next we will see how these differences are reflected in the quantitative analysis. Figure 4.8 shows the structure factors corresponding to Figures 4.3b and d, i.e., three-dimensional lamellar and spherical structures. There are several observations one can make based on the structure factors. First, the characteristic wave length is the same in both plots as it should be due to the selection of parameters. Second, the difference in magnitude is three decades in favor of the spherical structures, which reflects the robustness of the droplets. Third, there are more wave vectors forming the droplet structure as can be seen from the difference in the widths of the peaks. Fourth, the peaks are located approximately at $k = 2.2$, which is not very close to $k = 0.84$, as predicted by the linear analysis.

The structure factor shown in Figure 4.9 combines quantitatively the characteristics, which can be qualitatively seen in Figure 4.6b, i.e., the lamellar and spherical structures. If one compares the structure factors in the Figure 4.8 to the one in Figure 4.9, one can see that in Figure 4.9 the magnitude is between the magnitudes observed in pure droplets or lamellae. In addition, it can be seen that the lamellar structures dominate, since $S(k)$ is not as smooth as in the case of pure spherical droplets. This observation agrees with Figure 4.6b, where existence of quadratic in-

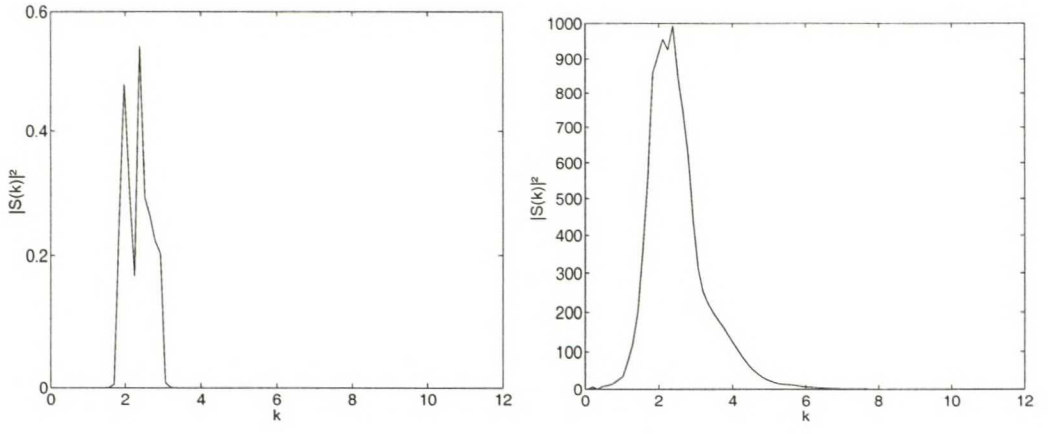

Figure 4.8: Structure factors of the lamellar and spherical structures with $k = 0.84$ (Figs. 4.3b and d). The structure factors were averaged over 30 stable samples. Notice that the peaks in a and b are in the same position in the k-axis, i.e., the characteristic wave length is the same in both structures as it should based on the linear analysis.

teractions is illustrated in the form of round shapes, but the structure is essentially lamellar.

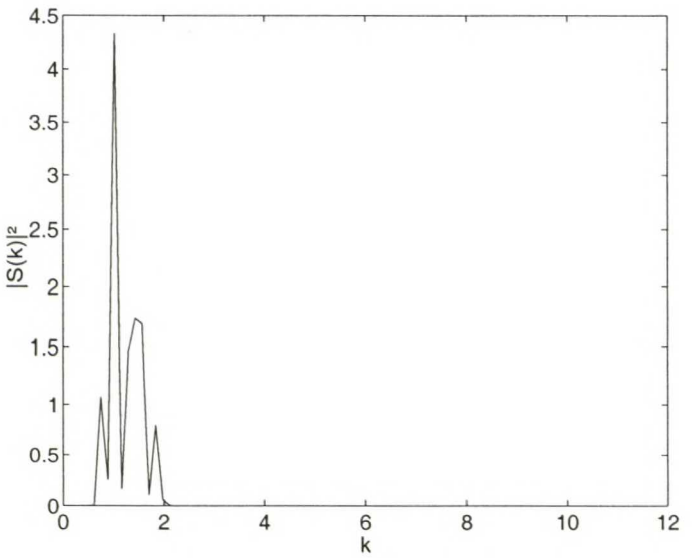

Figure 4.9: Structure factor of the competition of spherical and lamellar structures with $k = 0.45$ (Fig. 4.6b). The plot combines quantitatively the characteristics of the two cases in Figure 4.8.

Chapter 5

Gray-Scott model

This chapter concentrates on a more complicated reaction-diffusion system which describes irreversible chemical reactions. First, we show how reaction kinetics can be determined from formulae of chemical reactions. We will use linear analysis to predict the behavior of the system in the same manner as in previous chapter. When sources of chemicals are added to the system we can observe dendritic growth. Finally, we will propose a biological model, which is based on the Gray-Scott system.

5.1 The model

The second system we have studied is the Gray-Scott [Gray and Scott, 1983] model that was proposed to describe two irreversible autocatalytic chemical reactions. Autocatalysis means that the probability of occurrence of some morphology or chemical increases as a function of the number of such morphologies or the concentration of the chemical already present system. The reaction we want to describe is of the following form

$$\begin{aligned} \mathrm{U} + 2\mathrm{V} &\rightarrow_{r_1} 3\mathrm{V} \\ \mathrm{V} &\rightarrow_{r_2} \mathrm{P}, \end{aligned} \tag{5.1}$$

i.e., the reaction of one unit of chemical U and two units of V produces autocatalytically three units of V. Due to the irreversible nature of the reactions, chemical P is an inert product. In the reaction formula parameters r_1 and r_2 stand for the

reaction rate constants. In order to write down the differential equations for the process, it is assumed that the system is in contact with a reservoir of chemical U with a constant rate F and that chemical V is removed from the system by the feed process and in addition chemical V is converted to P with rate K. When we collect this, we obtain reactions

$$\begin{aligned} \mathrm{U} + 2\mathrm{V} &\rightarrow_1 3\mathrm{V} \\ \mathrm{V} &\rightarrow_K \mathrm{P} \\ \mathrm{V} &\rightarrow_F 0 \\ \mathrm{U} &\rightleftharpoons_F 0. \end{aligned} \tag{5.2}$$

According to the law of mass action (e.g. [Murray, 1993]), in chemical reactions the rate of reaction is proportional to the product of concentrations of reactants. We shall denote the concentrations by $u = [U]$ and $v = [V]$. Now we can write the reaction kinetics for the chemicals u and v as

$$\begin{aligned} f(u,v) &= -uv^2 + F - Fu = -uv^2 + F(1-u) \\ g(u,v) &= -2uv^2 + 3uv^2 - Fv - Kv = uv^2 - v(F+K). \end{aligned} \tag{5.3}$$

The equations of motion for the concentrations of the two chemicals $u \equiv u(\vec{x},t)$ and $v \equiv v(\vec{x},t)$ in dimensionless units can be obtained by substituting Eq. (5.3) into the general form of Turing system (Eq. (4.1)). This operation yields

$$\begin{aligned} u_t &= D_u \nabla^2 u - uv^2 + F(1-u) \\ v_t &= D_v \nabla^2 v + uv^2 - (F+K)v, \end{aligned} \tag{5.4}$$

where the diffusion coefficients for the two chemicals are D_u and D_v, respectively.

The Gray-Scott model was studied analytically and numerically in two dimensions, by Pearson [1993, see also http://www.cacr.caltech.edu/ismap/image.html], who mapped the phase diagram of the system in terms of the rate constants F and K. This model exhibits a very rich behavior ranging from time-independent steady-state solutions to chaotic, oscillatory, and to time-dependent phase turbulent behavior. Furthermore, [Vastano et al., 1987] have shown that the system develops spatially steady patterns even when the diffusion constants of the two chemicals are equal. This behavior is particular to the one-dimensional case and it has not been observed in higher dimensional systems.

In this study, we first performed numerical simulations of the Gray-Scott model in three dimensions. After that, we randomly added a small number sources for chemical V. The motivation for adding the sources was to investigate the robustness of patterns and the formation of connections between the sources in an attempt to mimic the development of a biological network, e.g., the formation of synaptic contacts between neurons. However, it is yet unclear whether Turing systems can produce such an inductive signaling mechanism for neural patterning but the idea is nevertheless appealing.

5.2 Linear analysis

As was already discussed in the previous chapter, the purpose of the linear analysis is to predict the stability and characteristics of the growth in a system. Turing showed that under certain conditions for the parameters, without diffusion a steady-state could be linearly stable, but in the presence of diffusion unstable. The parameters of the Turing system span a parameter space also known as Turing space. In some subdomain of this space we can create suitable circumstances for diffusion-driven instability. Our system is given as

$$\begin{cases} u_t = D_u \Delta u - uv^2 + F(1-u) \\ v_t = D_v \Delta v + uv^2 - (F+K)v. \end{cases} \tag{5.5}$$

Pearson [1993, see also http://www.cacr.caltech.edu/ismap/image.html] has analyzed this model and mapped the phase diagram of the system. By setting time variation and the diffusion terms to zero and solving the equations we get

$$v_0 = \frac{F(1-u_0)}{F+K}. \tag{5.6}$$

Fixing $u_0 = 1$ yields the steady-state solution $(u_0, v_0) = (1, 0)$. By substituting Eq. (5.6) back to the reaction terms of Eq. (5.5) we obtain another steady-state solution defined by Eq. (5.6) and

$$u_0 = \frac{1 \pm \sqrt{1 - \frac{4(F+K)^2}{F}}}{2}. \tag{5.7}$$

By the same kind of treatment as in the previous section and by using trial solutions defined by Eqs. (4.6) and (4.7) we can write Eq. (5.5) in the linearized form

$$\mathbf{w}_t = D\Delta\mathbf{w} + A\mathbf{w}, \tag{5.8}$$

where

$$\mathbf{w} = \begin{pmatrix} u - u_0 \\ v - v_0 \end{pmatrix},$$

$$D = \begin{pmatrix} D_u & 0 \\ 0 & D_v \end{pmatrix},$$

$$A = \begin{pmatrix} f_u & f_v \\ g_u & g_v \end{pmatrix},$$

with the following short-hand notations

$$f_u = -v_0^2 - F \tag{5.9}$$

$$f_v = -2u_0v_0 \tag{5.10}$$

$$g_u = v_0^2 \tag{5.11}$$

$$g_v = 2u_0v_0 - (F + K). \tag{5.12}$$

Now the dispersion relation is solved from

$$|\lambda I - A + Dk^2| = 0, \tag{5.13}$$

which stands for

$$\begin{vmatrix} \lambda - f_u + D_u k^2 & -f_v \\ -g_u & \lambda - g_v + D_v k^2 \end{vmatrix} = 0.$$

For the steady-state solution $(u_0, v_0) = (1, 0)$ we can easily solve the characteristic polynomial by calculating the determinant. The zeros of the characteristic polynomial, i.e., the eigenvalues are given as

$$\lambda_1 = -D_u k^2 - F, \ \lambda_2 = -D_v k^2 - F - K. \tag{5.14}$$

Both the eigenvalues are negative, which predicts in the sense of linear analysis that the steady-state $(1,0)$ does not bifurcate, i.e., there will be neither growth nor characteristic length scale in the system. $\lambda_1(k)$ is plotted in Figure 5.1 (solid line), where one can notice that $\lambda_1(k)$ does not bound any positive modes as the two other dispersion relations in Figure 5.1.

For the nontrivial steady-state defined by Eqs. (5.6) and (5.7) the calculation of the determinant yields the following characteristic polynomial

$$\lambda^2 + \lambda(v_0^2 - K + k^2(D_u + D_v)) + h(k^2), \tag{5.15}$$

where

$$h(k^2) = D_u D_v k^4 + (D_v(v_0^2 + F) - D_u(F + K))k^2 + (F + K)(v_0^2 - F). \tag{5.16}$$

Due to the form of the characteristic equation, it is hard to solve and we cannot follow the procedure we used in the steady-state case $(u_0, v_0) = (1,0)$. However, we can evaluate the critical wave vector by noticing that the region with positive $\lambda(k)$ in phase space is bounded by the the points given by zeros of $h(k^2)$. Because we want to isolate as few modes as possible we concentrate to the case in which $h(k^2)$ has only one zero. This occurs when the discriminant is zero, i.e.,

$$(D_v(v_0^2 + F) - D_u(F + K))^2 - 4D_u D_v(F + K)(v_0^2 - F) = 0. \tag{5.17}$$

If this relation is satisfied, the solution of Eq. (5.16) and the critical wave vector is given by

$$k_c^2 = \frac{D_u(F + K) - D_v(v_0^2 - F)}{2D_u D_v}. \tag{5.18}$$

The dispersion relations illustrating the window of wave vectors for the growing modes of the two selected phases are presented in Figure 5.1. The critical wave vector defined by Eq. (5.18) gives the k value corresponding to the maximum value of $\lambda(k)$, i.e., the most unstable growth mode. One should notice that in the case of the Gray-Scott model the number of allowed modes is larger than in the case of the general Turing system.

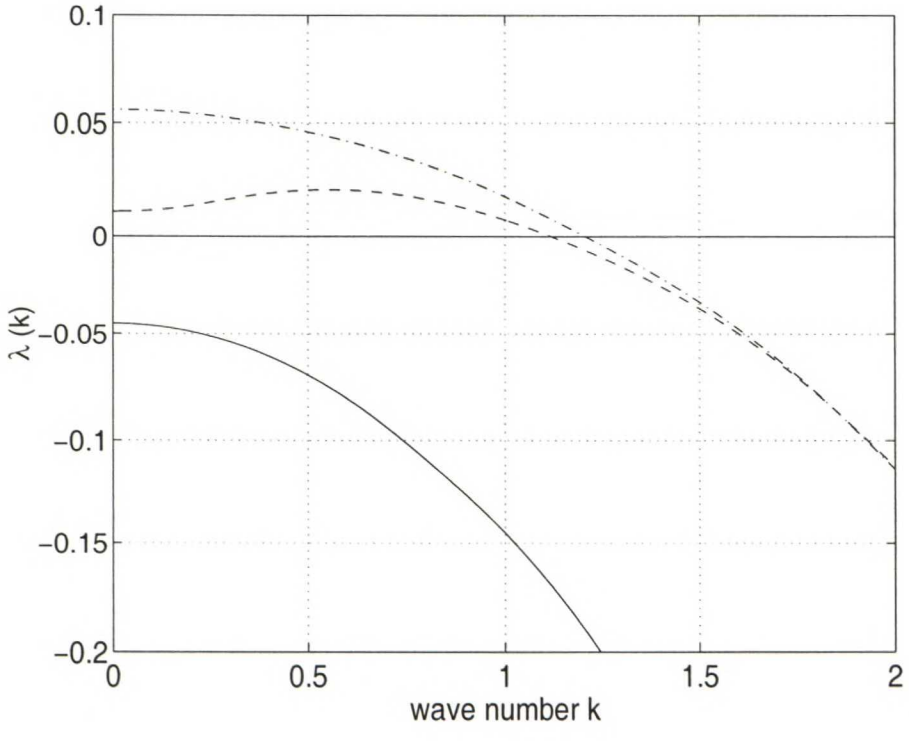

Figure 5.1: The dispersion relation of the Gray-Scott model for $D_u = 0.125$, $D_v = 0.05$, $F = 0.045$, $K = 0.065$ near the steady-state solution $(u_0, v_0) = (1, 0)$ (solid line), and $F = 0.065$, $K = 0.0625$ (dashed line) and $F = 0.045$, $K = 0.065$ (dash-dot line) near the nontrivial steady-state solution. The area above k-axis bounds the growing eigenmodes.

5.3 Simulation results

In this section, we will show that the Gray-Scott model produces complex tubular structures when sources of morphogen are added to the original system. We will also discuss its biological implications for modeling neuronal growth in more detail and show some preliminary results.

5.3.1 Dendritic growth

Using the Gray-Scott model of Eq. (5.4) we performed the simulations in two and three dimensions. By scanning the phase space we obtained very rich behavior. However, the results and especially the time dependence of some of the solutions caused difficulties in visualizing the resulting patterns in three dimensions. Thus the treatment of the Gray-Scott model is quite light here, but a systematic study of the properties of the Gray-Scott model in three dimensions is underway. However, it can be said that the three-dimensional Gray-Scott model displayed both disordered lamellar-like and droplet-like phases.

In the simulations presented here we have used $D_u = 0.125$ and $D_v = 0.05$ for the two diffusion constants and chose the parameters from the part of the phase space that can produce stripes. In this study we focused on the special case in which sources of chemical V were distributed randomly in the system. These sources feed the chemical to the system with a constant rate (+0.01). The shape of these sources is initially cross-like, having six branches in three dimensions to x, y and z-directions, respectively. For clarity, see Figure 5.2 where the growth of dendrites is simulated in two dimensions. Notice that the dendrites, indeed, seem to connect the sources of V.

As mentioned before, the motivation for including the sources is to investigate if the Turing mechanism could be considered as a candidate for describing neuronal growth. Should that be the case, the sources can be thought representing neurons which the growing dendrites must connect. In the sense of pattern formation in 3D systems, one requirement is the formation of stable tubular patterns. The Gray-Scott model clearly produces them in both two and three dimensions, see Figure 5.3. The connectedness of the three-dimensional network cannot be checked by visual analysis. However, based on the extensive two-dimensional simulations, we believe

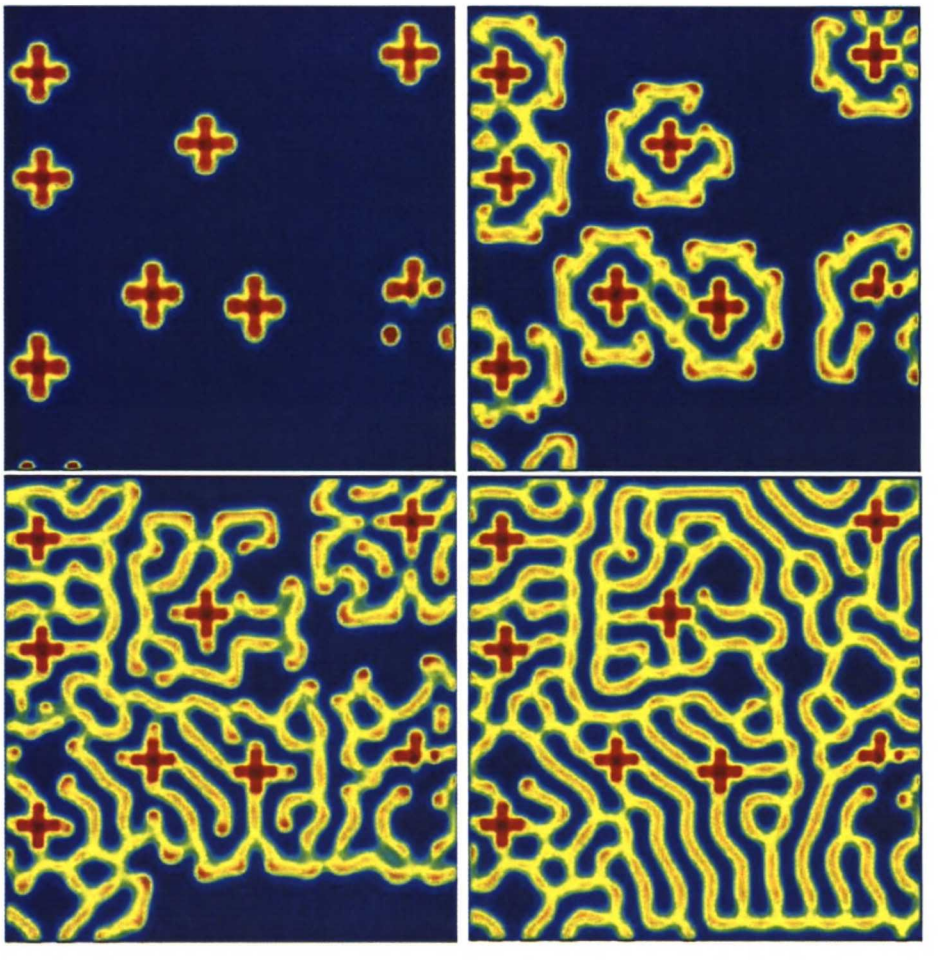

Figure 5.2: The growth of dendrites in a Gray-Scott model. The parameters were chosen to activate the phase producing stripes. There are eight sources of both U and V in the system.

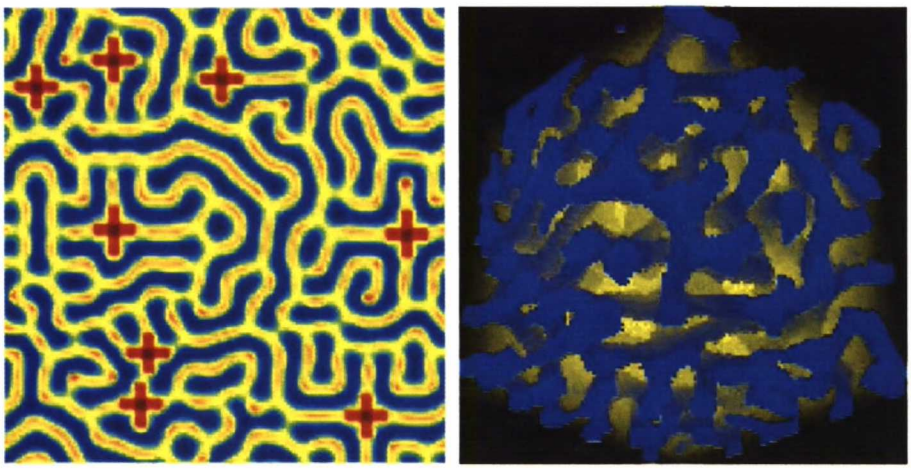

Figure 5.3: a) Pattern obtained in a 120×120 lattice with periodic boundary conditions using the two-dimensional Gray-Scott model in the presence of eight sources of morphogen V with parameters $F = 0.065$, $K = .0625$, $D_u = 0.125$, $D_v = 0.05$. The sources appear as cross-like patterns. b) Pattern obtained using the three-dimensional Gray-Scott model with four sources of V, $F = 0.045$, $K = 0.065$, $D_u = 0.125$, $D_v = 0.05$.

that the sources are connected by dendrites also in three dimensions.

The appearance of the tubular shapes seems characteristic for the Gray-Scott model whereas it was difficult to obtain in the case of the general Turing system. Figure 5.4 shows the structure factor of the three-dimensional structure with fully grown dendrites. One should notice that $S(k)$ is quite similar to the one calculated for the lamellar structure in section 4.4 (Figure 4.8a). However, the amplitude is one order of magnitude smaller in the case of Gray-Scott model.

5.3.2 Biological motivation

The Turing systems have been proposed to account for many patterns found on living creatures and organisms, e.g. fish [Barrio et al., 1998] [Painter et al., 1999], butterflies [Sekimura et al., 2000], sea urchins [Barrio et al., 1997] and viruses [Varea et al., 1999]. Also Murray [1993] discusses about coat patterning and asks rhetorically: "How leopard got its spots?". As Turing was once asked about the possibilities of his morphogenetic model and whether it could explain the stripes on a zebra, Turing allegedly responded: "The stripes are easy, it's the horse part that troubles me!". In the following we will study "the horse part" and introduce our model for describing

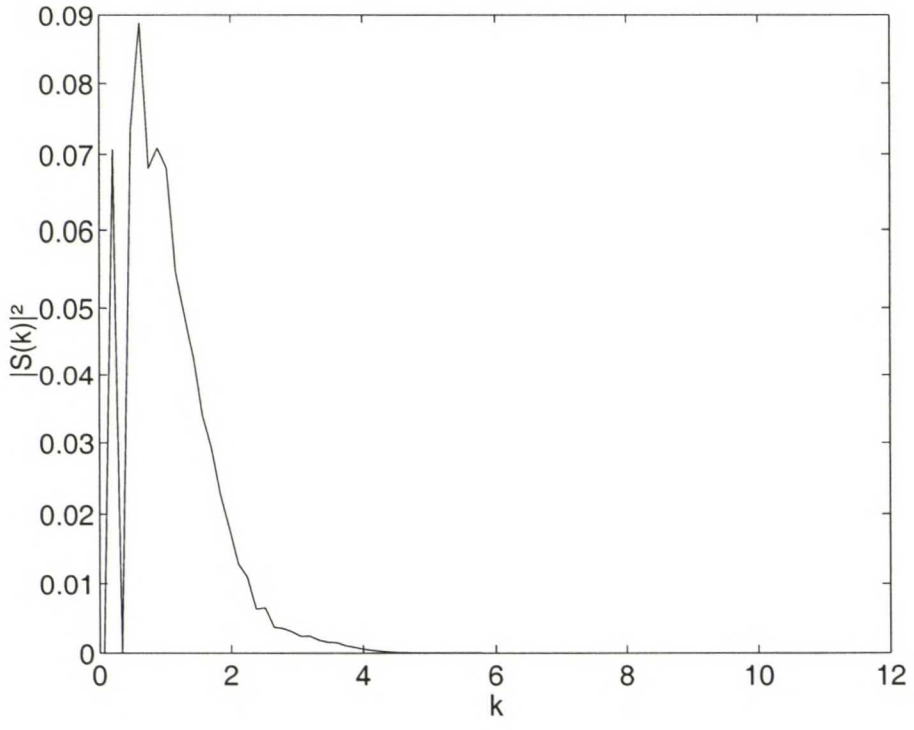

Figure 5.4: The structure factor corresponding to Figure 5.3b. Averaged over 30 samples.

some features of neural patterning.

Two distinct stages in the development of connections between neurons have been separated: super-innervation and elimination of axons. The former means establishing connections between neurons based on navigation by neurotrophic factors and the latter the optimization of the produced network by eliminating double connections, loops etc. It is known that the neurons do not always connect with their nearest neighbors, but can connect to other neurons very far. This kind of spatial selectivity cannot be explained by any model based on simple diffusion. Thus we propose Turing's reaction-diffusion to model such a neural patterning.

To model the optimization of the neural network we use a random walker model. Random walker models are widely used in simulating non-equilibrium phenomena and they have a connection to Turing systems in the sense that a memoryless random walk is actually a diffusion process. When we add some conditions for example how the walker reacts based on the "landscape" defined by the morphogen concentrations we obtain, in a sense, a discrete reaction-diffusion model. It is just easier to build discrete model than a continuous one for certain purpose. For an introduction to

random walker models see [Lam and Pochy, 1993].

The model we are currently studying is based on a walker model that has been used to simulate the trail formation of ants [Schweitzer et al., 1997]. Due to the fact that the development phase is still going on we will not go into details of our modified model, but give a general overview of the idea. We propose that the connections in the network produced by the Turing system act as signaling paths for chemicals responsible for diluting the network. These chemicals are simulated by using a random walker model in which we send a walker at a time from one neuron (nest). Then the walkers can walk only on the paths determined by the Turing pre-pattern and they drop pheromone (a chemical). When the walkers randomly find another neuron, they return to the nest based on sensing the pheromones. In the nest they recruit new walkers to strengthen the connection to the other neuron, which can be found based on another pheromone. The connections are formed based on the pheromones which the walkers leave behind. As the concentration of pheromone on a certain path exceeds some threshold value, i.e., many walker use the same route, a new connection arises.

It should be noted that although our model seems quite complex and sophisticated, it is in fact memoryless and can thus be used as a model for diffusion. The action of a walker at certain time is dependent only on its current position, not on the previous route it has taken. This condition is widely known as Markov condition. Another point is that everything in the system happens "on average". It is likely that the walker finds its way to the nest or to the neuron, but it is not certain. Thus we have to use many walkers to make the statistical probability of success high enough.

A preliminary result obtained using this model can be seen in Figure 5.5. The results are encouraging, but not perfect in any sense. The connections are clearly much more selective than in the original network. However, all the neurons are not connected to each other. The model is very complex and thus the details require more work. This research will be continued in the future.

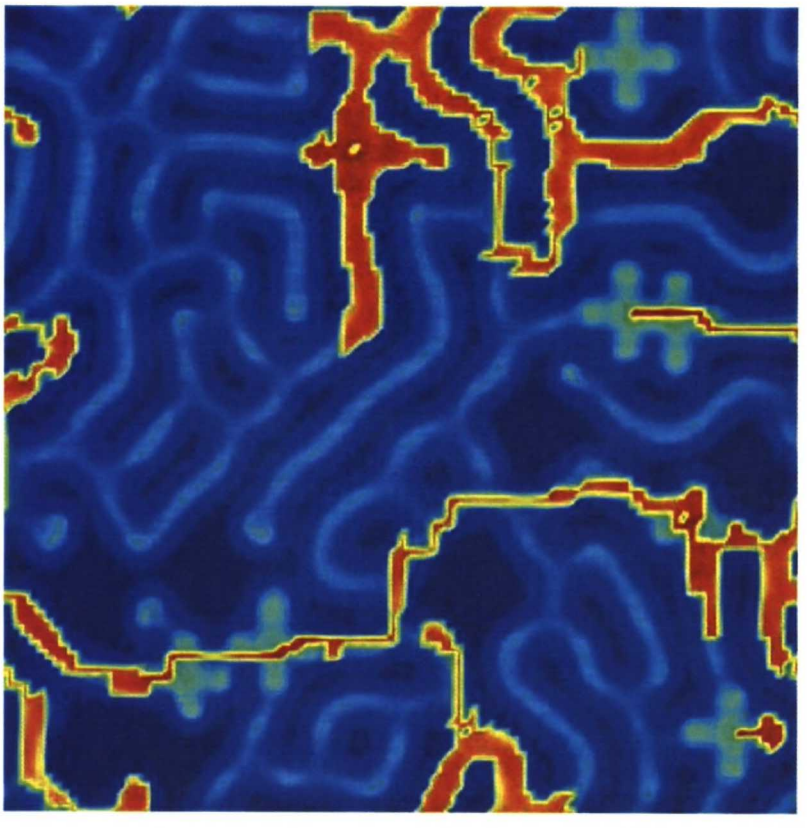

Figure 5.5: The result obtained by combining a random walker model to a Turing system. Notice that the connections become must simpler and clearer. The original network produced by Turing system can be seen on the background.

Chapter 6

Summary and Conclusions

In this thesis, we have studied two-dimensional spatial patterns and three-dimensional structures generated by a reaction-diffusion mechanism. A Turing system consists usually of two coupled reaction-diffusion equations. These equations describe the temporally varying concentration fields of chemicals called morphogens and they consist of a diffusion term and a reaction term. In these systems the reaction is always nonlinear, which results in the pattern formation behavior.

We introduced the basic concepts related to the pattern formation and showed examples of pattern formation observed in experiments. The pattern formation was discussed in three different systems: In a fluid between two plates with a temperature difference (Rayleigh-Bénard convection) and on a thin water layer lying on a vibrating plate (Faraday experiment). In these two systems, there are different pattern formation mechanisms and none of the above experiments is directly connected to the Turing mechanism. Thus, we discussed the first Turing-type chemical pattern in an open gel strip reactor.

Due to the nature of the Turing systems, they cannot be solved analytically, and thus one has to resort to numerical methods. The problem must be transformed into a discretized form and solved within the numerical error. The Turing systems are quite stable against random noise and thus the discretization error did not cause problems. The visualization was challenging due to the four-dimensionality of the data, but we found two methods for visualization.

The general Turing system we studied is phenomenological in the sense that we chose the reaction terms in such a way that we can enhance quadratic or cubic

interactions, corresponding to spots and stripes in two dimensions or droplets and lamellae in three dimensions. We carried out linear analysis to predict which modes will grow and dominate with certain parameter values. We compared the results of two- and three-dimensional systems and noticed that while spots and droplets are qualitatively similar in both two and three dimensions, two-dimensional stripes become lamellar structures in three dimensions. These lamellar structures show more defects than the stripe patterns in two dimensions.

As we used appropriate manipulative initial conditions, we could increase the regularity of the results and decrease the number of defects. By introducing one of the morphogens only to the mid-plane we obtained parallel planes, which is the most desirable ("minimum energy") structure of the lamellae and was not observed while the initial conditions were purely random. We could also drive droplet structures to hexagonal symmetry by using special initial conditions. More complex and irregular structures were obtained in two different ways: by allowing competition between nonlinear interactions or by allowing many different positive modes to grow.

The effect of noise on Turing structures had never before been studied. We used additive noise which was added at every time step, and perturbative noise which was used for analyzing the stability of the final structure. Based on the results we can conclude that spotty structures are much more stable than the lamellar structures. The stability against noise is a very important quality for morphogenetic models and these issues will be studied in the future from the developmental point of view, i.e., whether the noise makes it easier for the system to overcome meta-stable states and stabilize more quickly.

Another issue that is very interesting from the morphogenetic point of view is the effect of the size of the domain. We studied a system where the length of one side of the simulation box was increased between simulations. We noticed that the transition between the two and three dimensions took place as the characteristic wave length of the eigenmode equals the smallest dimension of the simulation box.

The other system we studied was the Gray-Scott model. This model is based on irreversible reactions of chemicals and we showed how it can be derived from chemical reaction formulae. We showed that as sources of the activator chemical are added, they become connected by a robust network in two dimensions. In the three-dimensional case we can clearly observe similar dendritic growth. However, the connectedness of the network remains to be studied in detail.

We proposed a model for modeling the growth of neural network by using a random walker model together with the Gray-Scott model. Such a united model has a plausible biological basis and preliminary results are promising, but the model requires much more work. In the future, we will concentrate on different kinds of growth models and other problems with a biological basis.

Bibliography

Neil W. Ashcroft and N. David Mermin. *Solid State Physics.* Saunders College Publishing, 1976.

R.A. Barrio, J.L. Aragon, C. Varea, M. Torres, I. Jimenez, and F. Montero de Espinosa. Robust symmetric patterns in the faraday experiment. *Physical Review E*, 56:4222–4230, 1997.

R.A. Barrio, C. Varea, J.L. Aragon, and P.K. Maini. A two-dimensional numerical study of spatial pattern formation in interacting turing systems. *Bulletin of Mathematical Biology*, 61:483–505, 1998.

H. Bénard. *Revue Générale des Sciences Pures et Appliques*, 11:1261, 1900.

V. Castets, E. Dulos, J. Boissonade, and P. De Kepper. Experimental evidence of a sustained standing turing-type nonequilibrium chemical pattern. *Physical Review Letters*, 64:2953–2956, 1990.

M.C. Cross and P.C. Hohenberg. Pattern formation outside of equilibrium. *Reviews of Modern Physics*, 65:851–1112, 1993.

J. Paul Devlin. Ice, discovery channel school, original content provided by world book online. *http://www.discoveryschool.com/*, cited 15.11.2001.

Michael Faraday. *Philosophical Transactions of Royal Society London*, 121:299, 1831.

Matteo Frigo and Steven G. Johnson. *http://www.fftw.org/*, cited 5.12.2001.

P. Gray and S.K. Scott. Autocatalytic reactions in the isothermal continuous, stirred-tank reactor: isolas and other forms of multistability. *Chemical Engineering Science*, 38:29–43, 1983.

John W. Harris and Korst Stocker. *Handbook of Mathematics and Computational Science.* Springer, 1998.

Mikko Karttunen. unpublished. 2001.

Mikko Karttunen, Nikolas Provatas, Tapio Ala-Nissila, and Martin Grant. Nucleation, growth and scaling in slow combustion. *Journal of Statistical Physics*, 90: 1401–1411, 1997.

Lui Lam and Roccho Pochy. Active-walker models: Growth and form in nonequilibrium systems. *Computers in Physics*, 7:534–541, 1993.

Marsaglia and Zaman. *FSU-SCRI-87-50*, 1987.

J.D. Murray. *Mathematical Biology, second edition.* Springer-Verlag, 1993.

Ville Mustonen. *Parallel molecular dynamics simulation of solid materials.* M.Sc. thesis, Helsinki University of Technology, 2001.

G. Nicolis. *Introduction to nonlinear science.* Cambridge University Press, 1995.

K.J. Painter, P.K. Maini, and H.G. Othmer. Stripe formation in juvenile pomathancus explained by a generalized turing mechanism with chemotaxis. *Proceedings of National Academy of Science USA*, 96:5549–5554, 1999.

John E. Pearson. Complex patterns in a simple system. *Science*, 261:189–192, 1993, see also http://www.cacr.caltech.edu/ismap/image.html.

John E. Pearson. Citation histogram of turing's article. *http://www-xdiv.lanl.gov/XCM/pearson/*, cited 26.7.2001.

William H. Press, Saul A. Teukolsky, William T. Wtterling, and Brian P. Flannery. *Numerical Recipes in C.* Cambridge University Press, second edition, 1995.

N. Provatas, T. Ala-Nissilä, M. Grant, K.R. Elder, and L. Piché. Scaling, propagation, and kinetic roughening of flame fronts in random media. *Journal of Statistical Physics*, 81:737–759, 1995.

M.I. Rabinovich, A.B. Ezersky, and P.D. Weidman. *The Dynamics of Patterns.* World Scientific, 2000.

Lord Rayleigh. *Phil. Mag.*, 32:529, 1916.

Frank Schweitzer, Kenneth Lao, and Fereydoon Family. Active random walkers simulate trunk trail formation by ants. *BioSystems*, 41:153–166, 1997.

Toshio Sekimura, Anotida Madzvamuse, Andrew J. Wathen, and Philip K. Maini. A model for colour pattern formation in the butterfly wing of papilio dardanus. *Proceedings Royal Society London B*, 267:851–859, 2000.

J. Swift and P.C. Hohenberg. Hydrodynamic fluctuations at the convective instability. *Physical Review A*, 15:319, 1977.

A.M. Turing. The chemical basis of morphogenesis. *Philosophical Transactions of Royal Society London*, B237:37–72, 1952.

C. Varea, J.L. Aragon, and R.A. Barrio. Turing patterns on a sphere. *Physical Review E*, 60:4588–4592, 1999.

J.A. Vastano, J. E. Pearson, W. Horsthemke, and H.L. Swinney. *Physics Letters A*, 124:6, 1987.